5

Defected and Substitutionally Doped Nanotubes: Applications in Biosystems, Sensors, Nanoelectronics, and Catalysis

Charles See Yeung, Ya Kun Chen and Yan Alexander Wang
Department of Chemistry, University of British Columbia, Vancouver, Canada

1. Introduction

Carbon nanotubes (CNTs) have been the subject of intensive research since their discovery by Iijima in the early 1990s (Iijima 1991). Single-walled carbon nanotubes (SWCNTs, Iijima & Ichihashi 1993; Bethune et al. 1993) are of particular interest because the electronic properties of these nanomaterials can vary from semiconducting to metallic depending on its molecular structure. This contrasts multi-walled carbon nanotubes (MWCNTs), which are metallic and exhibit a zero bandgap. Fundamental understanding of these supramolecular carbon allotropes (Tasis et al. 2006; Ajayan 1999) is essential to the development of new nanomaterials for applications in biosystems, sensors (Wang & Yeow 2009; Hu & Hu 2009; Li et al. 2008), optics (Avouris 2008), nanomechanics (Li et al. 2008; Park 2004), nanoelectronics (Park 2004; Fuhrer 2003; Tsukagoshi 2002), and catalysis (Serp 2003, Tian et al. 2006, Yeung et al. 2011).

The molecular structure of SWCNTs can be described as a cylindrical roll of an infinite graphene sheet and is characterized by a chiral circumferential vector $\mathbf{AB} = ma + nb$, a linear combination of two unit lattice vectors a and b where m and n are integers (Figure 1-1, Ajayan 1999; Moniruzzaman & Winey 2006). The pair of indices (m,n) for any given nanotube determines its diameter, chirality, and electronic character. For all $n = m$, the nanotube is termed armchair and is metallic, exhibiting a zero bandgap. For $n \neq m$ and neither n and m are zero, the nanotube exhibits chirality and supramolecular helicity, having important implications in optical properties. For $n = 0$ or $m = 0$, the nanotube is termed zigzag. For $n - m = 3p$, where p is a non-zero integer, the nanotube is semimetallic with a band gap on the order of meV. For $n - m \neq 3p$, where p is a non-zero integer, the nanotube is semiconducting with a band gap on the order of 1 eV; as a general rule of thumb, the observed band gaps are roughly proportional to the reciprocal of the tube radius.

Each individual C atom in the sidewall of a CNT exhibits pyramidalization and partial sp^3 hybridization as a result of sidewall curvature. This phenomenon leads to a weakening of the overall π-conjugation of the SWCNT and slight misalignment of π-orbitals between adjacent atoms. Curved π-conjugation can be quantified using Haddon's π-orbital axis vector (POAV) method (Figure 1-2, Haddon & Scott 1986). In this analysis, the pyramidalization angle $\theta_p = \theta_{\sigma\pi} - 90^o$, where $\theta_{\sigma\pi}$ is the angle between the π-orbital and the σ-bond of the C atom of interest. In contrast to planar (i.e., $\theta_p = 0^o$) and pyramidal (i.e.,

θ_p = 19.5°) geometries, nanotubes exhibit varying degrees of pyramidalization depending on the tube diameter. In general, SWCNTs are more inert than corresponding fullerenes with similar diameters. Alternatively, Li introduced the concept of bond curvature K to better describe the supramolecular curvature of CNTs and offer more accurate predictions for chemical reactivity based on the local curvature of the independent C–C bonds (Li et al. 2007). K is characterized by directional curvature K_D (corresponding to the arc curvature of C−C bonds) and its mean K_M (corresponding to arc curvature of the vertex carbon atoms).

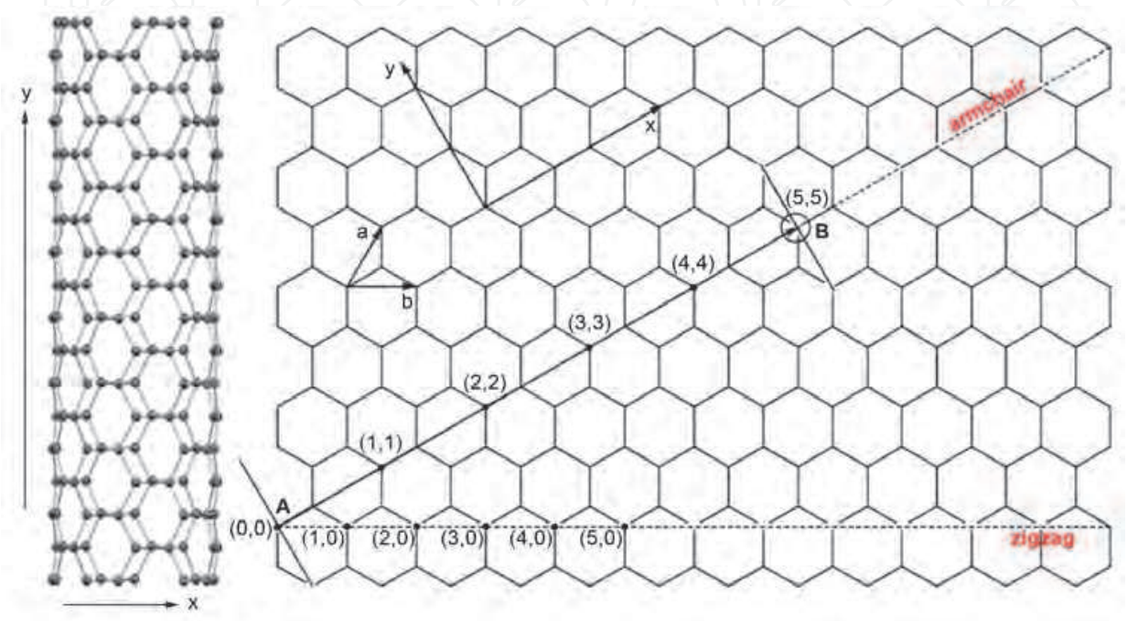

Fig. 1.1. A schematic drawing of graphene wrapping to form SWCNTs. The (5,5) SWCNT on the left is drawn highlighting wrapping vector x and translation vector y (Tian et al. 2006).

Carbon nanotubes are characterized by a very high aspect ratio (i.e., length per width) and display a very large surface area. Attractive interactions by van der Waals or weak long-range covalent bonding on the order of 0.50 to 0.95 eV per nanometer of tube-to-tube contact have been observed. Aggregation of CNTs often results in the generation of hexagonally packed bundles or ropes. SWCNTs exhibit extensive levels of electron delocalization and strong confinement effects that result in a pronounced one-dimensionality and weak interaction between electrons and phonons. These nanomaterials are ballistic conductors and exhibit two units of quantum conductance (i.e., $4e^2/h$) and mean free paths on the order of μm (Javey 2003; White 1998).

Natural carbon nanotubes can exhibit defects formed either during their synthesis or as a result of environmental stress that have significant effects on the geometric and electronic properties of carbon nanomaterials (Collins 2010; Charlier 2002). The most typical type of defects are point vacancies in which an atom is missing in the crystalline lattice of the nanotube backbone and occur as a result of external radiation (e.g., high energy electron, ion, or neutron radiation) in which a carbon atom is either dislodged or fully removed. A single vacancy of this type generates three dangling bonds (DBs) and immediately undergoes structural reorganization, for example, yielding the 5-1DB defect in which one five-membered carbocycle is formed, leaving a single C atom with a reactive DB (Berber &

Oshiyama 2006; Ajayan 1998). Different from point vacancies, other structural defects arising from geometric rearrangements may also be present in nanotube sidewalls. The simplest of these rearrangements is the pentagon-heptagon defect in which a single C–C bond positioned between two adjacent hexagon rings undergoes a simple bond rotation, resulting in the formation of two non-hexagonal rings. Pentagon-heptagon defects have minimal effect on the local environment of the nanotube but induce a global buckling of the macromolecule, leading to significant changes in conductivity and aggregation (Chico 2010; Sonia & Niranjan 2010). Of note, two adjacent pentagon-heptagon defects can form a pentagonal-heptagonal-heptagonal-pentagonal (5775) structure known also as the Stone-Wales (SW) defect (Stone & Wales 1986).

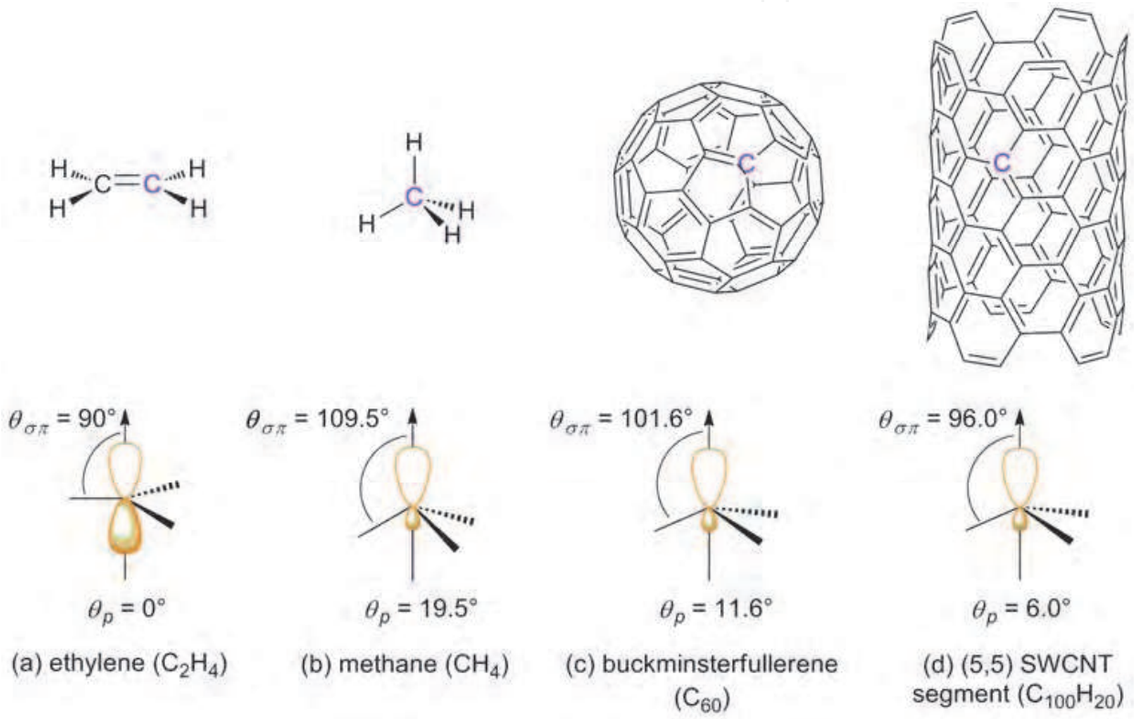

Fig. 1.2. π-orbital axis vector (POAV) analysis of curved π-conjugation in (a) ethylene, (b) methane, (c) buckminterfullerene, and (d) a (5,5) SWCNT segment (Yeung et al. 2011).

Chemical functionalization provides scientists an opportunity for fine-tuning the electrical properties of carbon nanotubes for the desired application. CNTs are known to exhibit interstitial defects, or extra atoms not present in a lattice site, as a result of atmospheric oxidation (Collins 2010). Covalent modification by treatment of these carbon macromolecules with chemical reagents has been accomplished (Karousis et al. 2010; Tasis et al. 2006). The chemical reactivity of nanotube sidewalls bears some resemblance to that of olefins (i.e., C=C double bonds). As such, strategies including ozonolysis, Diels-Alder cycloaddition, osmylation, hydroboration, carbene addition, nitrene addition, dipolar cycloaddition of azomethine ylides, and vinylcarbonylation via zwitterionic intermediates are possible. Other methods include fluorination followed by nucleophilic substitution, dissolving metal reduction (i.e., Billups reaction), electrophilic oxidations, and free radical reactions including alkylation, perfluoroalkylation, and arylation.

Direct substitutional replacement of a sidewall C atom with a heteroatom is another alternative for electronic tuning (Ewels et al. 2010; Glerup et al. 2010). Substitutional doping of a SWCNT produces a hetero-SWCNT (HSWCNT) that exhibits geometric and electronic properties distinct from pristine carbon nanotubes depending on the doping concentration. Replacement of a single C atom with N or B is of particular interest because of the generation of quasibound states consisting of *p*-orbitals above and below the Fermi energy, respectively, in analogy to *p*- and *n*-type semiconductors. This is because boron has one less electron than carbon, while nitrogen has one more electron. Both N- and B-doped SWCNTs have been synthesized by thermal treatment, chemical vapor deposition, laser ablation, and arc methods, but generally with poor control of doping position and concentration. Srivastava et al. predicted that a free gas-phase neutral N atom, if brought into close vicinity of a backbone vacancy defect, could induce a selective substitution to occur (Srivastava et al. 2004). Alternatively, our group proposed that nitrogen monoxide (NO) could be used as a nitrogen source by interaction with the 5-1DB defects (Liu et al. 2006). Substitutional doping, such as N-doping, typically causes minimal geometric changes in comparison to their undoped congeners.

Although physisorption of transition metals onto CNTs is a known process, substitutional doping in which the transition metal atom is embedded into the sidewall remains an unsolved challenge in nanoscience, although some researchers have proposed that this transformation may be assisted by the presence of vacancy defects (Yang et al. 2006; Zhuang et al. 2008). The corresponding transition metal substitutionally doped fullerenes, however, have been prepared experimentally and characterized (Branz et al. 1998; Poblet et al. 1999; Kong et al. 2003). For example, *d*-block transition metals Pt-, Ir-, Rh-, Sc-, and Y-, and *f*-block La- and Sm-doped fullerenes have been synthesized by laser ablation or ionization and can be detected by mass spectrometry. Although the mechanistic details concerning substitution are sparse, it is believed that a fullerene-transition metal adsorbate complex is formed as a result of strong interactions between the metal *d*-orbitals and extended π-framework of the fullerene, followed by direct insertion into the carbon framework (Changgeng et al. 2001). In some cases, the initial generation of vacancy defects may induce the observed structural rearrangement. The synthesis of second- and third-row transition metal-doped fullerenes has been predicted by the chemical reaction of transition metal chloride (MCl_n) with buckminsterfullerene (C_{60}) under an atmosphere of chlorine gas (Cl_2, Sparta et al. 2006).

Theoretical studies of transition metal-doped fullerenes suggest a decrease in the energy gap between the highest occupied molecular orbital (HOMO) and the lowest unoccupied molecular orbital (LUMO), leading to both higher conductivity and reactivity (Changgeng et al. 2001). As such, transition metal-doped SWCNTs may display enhanced electronic properties in comparison to their undoped analogs. The introduction of transition metals is an attractive prospect because of the inherently rich chemistry of transition metal surfaces and organometallic complexes. By adding *d*-orbitals to the extended π-framework of the C atoms, it may be possible to enhance the ability of nanotubes to interact and bind small adsorbates such as NO, a molecule critical to biological systems. Since coordination of transition metals affect the electronic nature of the metal center, it is possible that a HSWCNT containing a transition metal atom embedded in the sidewall of the nanotube may exhibit changes in conductance in the presence of gases such as carbon monoxide (CO), water (H_2O), and ammonia (NH_3). By monitoring current, the development of new nanosensors may be possible (Peng & Cho 2003; Sinha et al. 2006; Li et al. 2008; Rouxinol et al. 2010; Yeung et al. 2010). This prospect also has important implications in efforts toward

new nanoelectronic devices. Controlled storage, capture, activation, and release of other relevant molecules, including hydrogen (H_2), is another potential application of transition metal-doped SWCNTs based on the known reactivity of transition metals. We have also conducted preliminary investigations highlighting the similarity between transition metal-doped SWCNTs and simple alkyl complexes, suggesting that nanocatalysis (e.g., Lewis acid catalysis) may be optimal using sidewall substitution as the key strategy for immobilizing these metals (Yeung et al. 2007; Yeung & Wang 2011). Indeed, transition metal-doped SWCNTs could sit at the interface between heterogeneous and homogeneous catalysts and provide complementary reactivity to traditional systems.

Our work in SWCNTs and their substitutionally doped analogs (i.e., HSWCNTs) is driven by a fundamental interest in the unique chemical reactivity afforded by these macromolecules. We have focused our investigations primarily on defected and substitutionally doped nanotubes because of their potential applications in biological systems, sensory technology, nanoelectronics, and catalysis. In this account, we highlight our theoretical studies on the geometric and electronic structure of defected and doped SWCNTs, their chemical reactivity, and proposed applications of these nanomaterials. We also describe the related defected and doped boron-nitride nanotubes (BNNTs) and their behavior.

2. Models and computational details

We chose the (5,5) armchair metallic SWCNT and (5,0) zigzag SWCNT as models for all computations with suitable capping groups (i.e., either a fullerene hemisphere or H atoms). All calculations were done with Gaussian 03 (Frisch et al. 2003). Natural bond orbital (NBO) analysis was conducted with Gaussian NBO Version 3.1 (Reed et al. 1988) to obtain the frontier molecular orbitals (FMOs, Fukui 1982): the HOMO and the LUMO. Density of states (DOS) and local DOS (LDOS) studies were performed using PyMOlyze Version 1.1 (Tenderholt 2005). The Hessian was calculated to verify the nature of stationary points on the potential energy surface (PES, either a local minimum or transition state). Optimizations using spin-restricted and spin-unrestricted methods provided the same results.

To study the substitutional doping of SWCNTs, we envisioned a chemical reaction between a single vacancy defect on the backbone of the nanotube and a suitable atom transfer reagent. To this end, we evaluated the use of NO and ozone (O_3) for N- and O-substitutional doping, respectively. For N-doped SWCNT synthesis with NO (Liu et al. 2006), a single C atom was removed from the middle of a (5,5) segment capped with H atoms ($C_{199}H_{20}$), yielding a metastable conformation with three dangling bonds. Geometry optimization with semiempirical MNDO-PM3 method (Stewart 1989) and hybrid Hartree-Fock/density functional theory (DFT) method B3LYP (Becke 1988; Lee et al. 1988) using Pople's 6-31G basis set (Ditchfield et al. 1971) afforded the 5-1DB defect. To study the chemical reactivity, we employed a two-layer ONIOM (our own N-layered integrated molecular orbital and molecular mechanics) model (Dapprich et al. 1999), with the nine-membered ring surrounding the defect modeled with C_9H_8 as the higher layer at B3LYP/6-31G(d), while all other atoms were the lower layer treated with universal force field (UFF, Rappe et al. 1992). For O-doped SWCNT synthesis with O_3 (Liu et al. 2006b), an analogous system was used ($C_{119}H_{20}$). Geometry optimization was achieved with semiempirical AM1 (Dewar et al. 1985) and B3LYP/6-31G. Static quantum mechanical calculations were validated by the atom-centered density matrix propagation (ADMP) based *ab initio* molecular dynamics (AIMD) simulation (Schlegel et al. 2001)

To study transition metal-doped SWCNTs, we initiated our studies using one-dimensional periodic boundary conditions with 100 carbon atoms in the primitive cell (Chen et al. 2011). Replacement of a single C atom in the middle of the cell with a transition metal was performed, followed by geometry optimization with PBEPBE (Perdew et al. 1996) using LANL2DZ (Dunning Jr. & Hay 1976), Hay and Wadt's relativistic 18-electron Los Alamos National Laboratory effective core pseudopotential (ECP, Hay & Wadt 1985). We then focused our investigations on Pt due to its prevalence in well-defined organometallic complexes and heterogeneous catalysis. Two (5,5) models were chosen in which a C atom was substituted with Pt: 1) $C_{69}H_{20}Pt$ with H caps (Yeung et al. 2007; Yeung et al. 2010), and 2) C_{170} with D_{5h} symmetry and hemispherical caps (Tian et al. 2006). For $C_{69}H_{20}Pt$, DFT calculations were performed with PBEPBE using LANL2MB, followed by LANLDZ. For $C_{169}Pt$, we used BPW91 (Becke 1988; Perdew et al. 1996a). We also chose a (5,0) model containing of formula $C_{49}H_{10}Pt$ (Yeung & Wang 2011), optimized with B3LYP/LANL2DZ. NMR chemical shifts (δ) were calculated using the gauge-independent atomic orbital (GIAO) method (Wolinski et al. 1990). We further examined model Pt complexes. Alkylplatinum species $PtMe_3^+$ and its CO-adsorbates (i.e., with a C-end coordinated CO) was evaluated with PBEPBE. $PtMe_3^+$, $PtPh_3^+$, Pt-doped phenaline, Pt-doped sumanene, Pt-doped corannulene, and Pt-doped C_{24} fullerene (with Pt substitution at the junction between three pentagons being PPP and between a hexagon and two pentagons being HPP) were also considered with B3LYP/LANL2MB and LANL2DZ.

To study the importance of the carbon backbone, the isoelectronic transition metal-doped single-walled boron nitride nanotube (BNNT) and its undoped analog were investigated (Chen et al. 2010). Defected BNNT models containing SW defects (Stone & Wales 1986) had formula $B_{45}N_{45}H_{20}$, while Pt substitutional doping gave two isomers, $B_{44}N_{45}H_{20}Pt$ and $B_{45}N_{44}H_{20}Pt$. DFT calculations were performed using B3LYP/LANL2MB, followed by LANL2DZ.

3. Defected SWCNTs

3.1 Defected SWCNT rods

We investigated vacancy defects of SWCNTs by removing a single atom from the middle of model (5,5) SWCNT rod capped with H atoms ($C_{200}H_{20}$), yielding a defected SWCNT ($C_{199}H_{20}$) that undergoes subsequent structural rearrangement to the 5-1DB defect (Figure 3-1, Liu et al. 2006). In our model system, a single C atom protrudes to the exterior of the sidewall and is the active carbon (C1). Other than the nine C atoms surrounding the vacancy, the remainder C atoms in the hexagonal lattice remain relatively unaffected. Because of coordinative unsaturation and less steric hindrance, a higher chemical reactivity is expected. The electronic structure was affected by introduction of the defect, as determined by a decrease in HOMO−LUMO gap from 1.38 to 0.84 eV. The HOMO of the defected SWCNT contains a large contribution from the lone pair on the active carbon atom and the π-bonds of the other atoms surrounding the vacancy. We also determined that a smaller model system (C_9H_8) with fixed geometry can be used to represent most of the chemical properties of the defect by qualitative comparison of the FMOs. Introduction of the vacancy defect also resulted in several small changes in the DOS (Figure 3-2). We have also studied the effect of multiple vacancies and have observed related structural rearrangements (Liu et al. 2009).

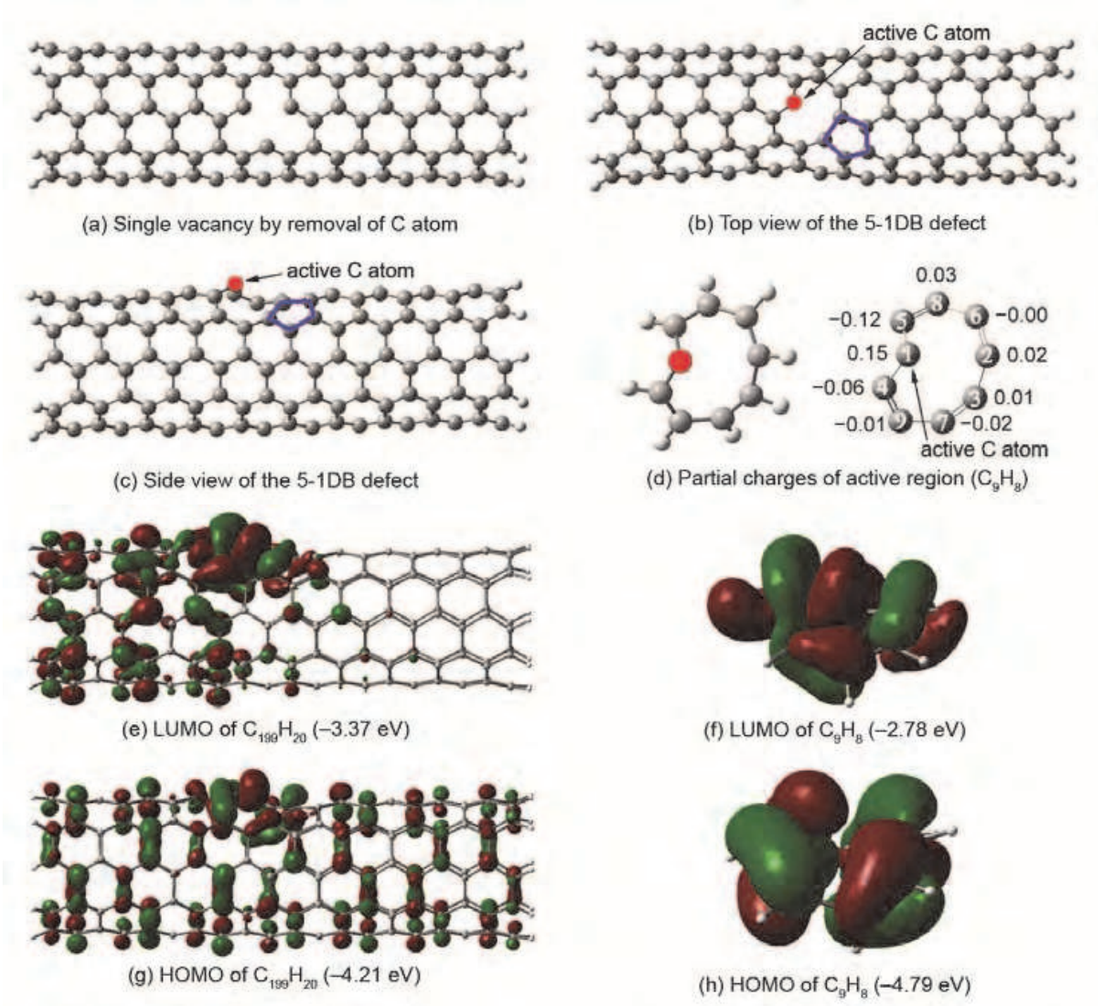

Fig. 3.1. Optimized geometry and FMOs of a 5-1DB defected SWCNT and higher-layer model C_9H_8. Orbital energies are in parentheses (Liu et al. 2006). Legend: dark grey = C, light grey = H.

3.3 Substitutional N-doping of SWCNTs via reaction with NO

Based on FMO analysis, the active carbon (C1) of the 5-1DB defect, expected to be reactive toward small molecules, contains an sp^2-orbital with 1.51 electrons, a p-orbital with 0.51 electrons, and an overall charge of 0.149 (Liu et al. 2006). As the first example, we chose nitrogen monoxide (NO) as the representative small-molecule reagent.

Nitrogen monoxide is of particular interest due to its biological relevance (Miller & Megson 2007). In fact, while NO has a reputation for destroying O_3, causing cancer, and fostering acid rain, it is a critical signaling molecule in biological systems, important for learning and memory, blood pressure regulation, skin homeostasis, inflammation, and carcinoma metastasis. As such, NO was named "Molecule of the Year" in 1992 (Culotta & Koshland Jr. 1992). Physiological NO is biosynthesized via a five-electron oxidation of the amino acid arginine (Figure 3-3) and can impact biosystems based on its ability to interact with molecular oxygen to yield reactive oxygen species (ROS) including hydroxyl radicals (HO•),

nitrogen dioxide (N_2O_4), and peroxynitrite ($ONOO^-$). Free NO exhibits polarization where the O atom bears a charge of −0.181, thus making chemical reactivity likely.

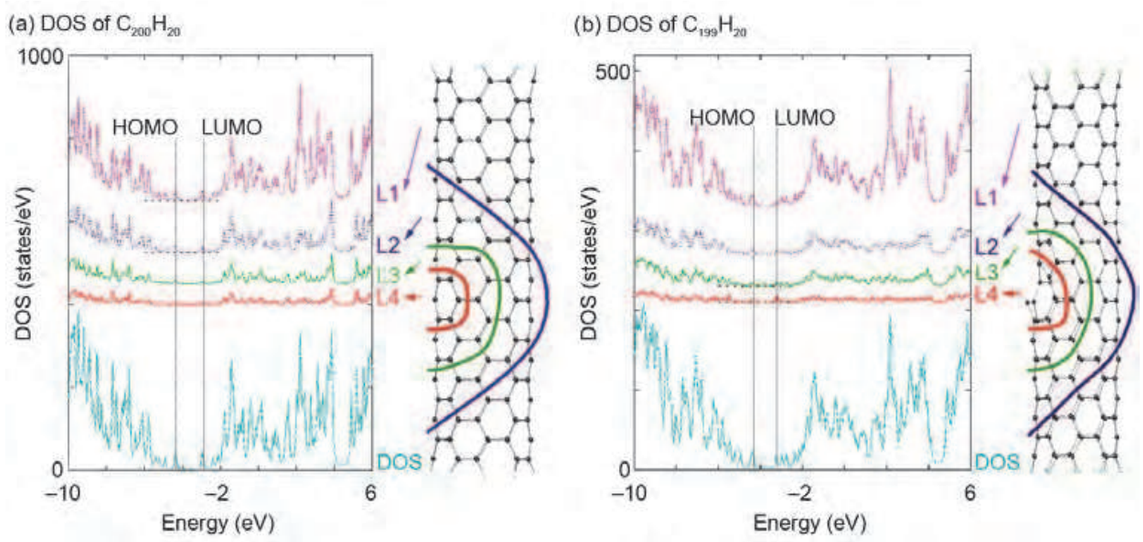

Fig. 3.2. Optimized geometries, DOS, and LDOS of (a) $C_{200}H_{20}$ (ε_{HOMO} = −4.35 eV, ε_{LUMO} = −2.97 eV) and (b) $C_{199}H_{20}$ (ε_{HOMO} = −4.21 eV, ε_{LUMO} = −3.37 eV). L1−L4 are the LDOS for the specified layer of atoms (Liu et al. 2006).

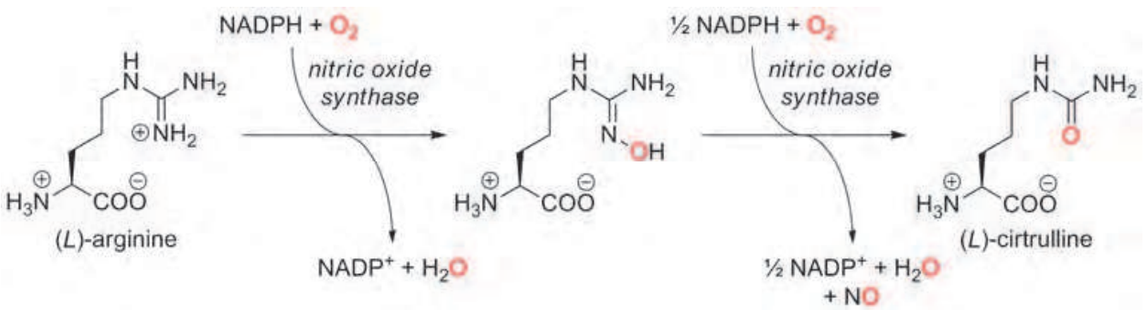

Fig. 3.3. Biosynthesis of NO from (*L*)-arginine (Griffith & Stuehr 1995).

The reaction of NO with the defected SWCNT proceeds in two distinct stages. First, an electrostatic interaction between the defected SWCNT and NO takes place, involving an O-end attack of NO onto the active C atom via an orbital interaction between the singly-occupied molecular orbital (SOMO) of NO and the HOMO of the SWCNT (Figure 3-4), producing heterocycle **INT1** containing an N−O bond. This rate-limiting step takes place rapidly with a low activation barrier (8.6 kcal/mol). Next, the N atom undergoes insertion into the nearby C2−C3 bond of the adjacent pentagon, expanding the pentagon via a three-membered transition state to liberate **INT2** containing a six-membered N-containing heterocycle. C1−N bond formation then occurs with concomitant cleavage of the C1−O bond to give **INT3**, formally an N-doped SWCNT that has undergone pyrimidalizing oxygenation where the N atom has filled the single vacancy where the C atom was removed (i.e., substitutional doping). The N−O bond is relatively weak, with a bond length of 1.41 Å and a

partial charge of −0.574 residing on the O atom. A second equivalent of NO initiates cleavage of this N−O bond via a four-membered concerted and asynchronous transition state, liberating one molecule of nitrogen dioxide (NO_2) and **Product**, the N-doped SWCNT ($C_{199}H_{20}N$), a thermodynamically feasible process (ΔE = 78.3 kcal/mol).

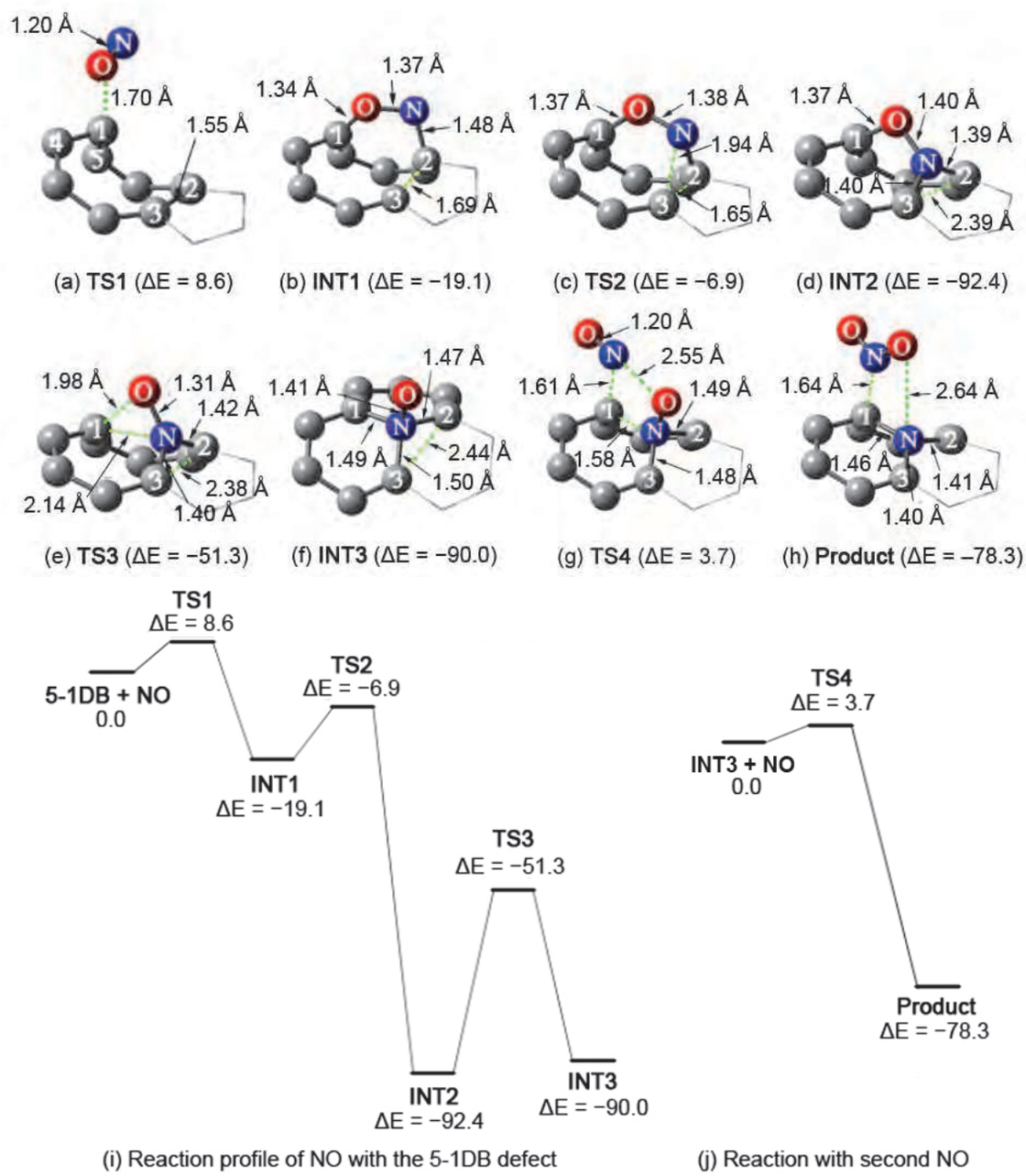

Fig. 3.4. Optimized geometries and energy profiles (with energies in kcal/mol) for the reaction of the defected SWCNT with NO (Liu et al. 2006). Legend: dark grey = C, navy blue = N, red = O.

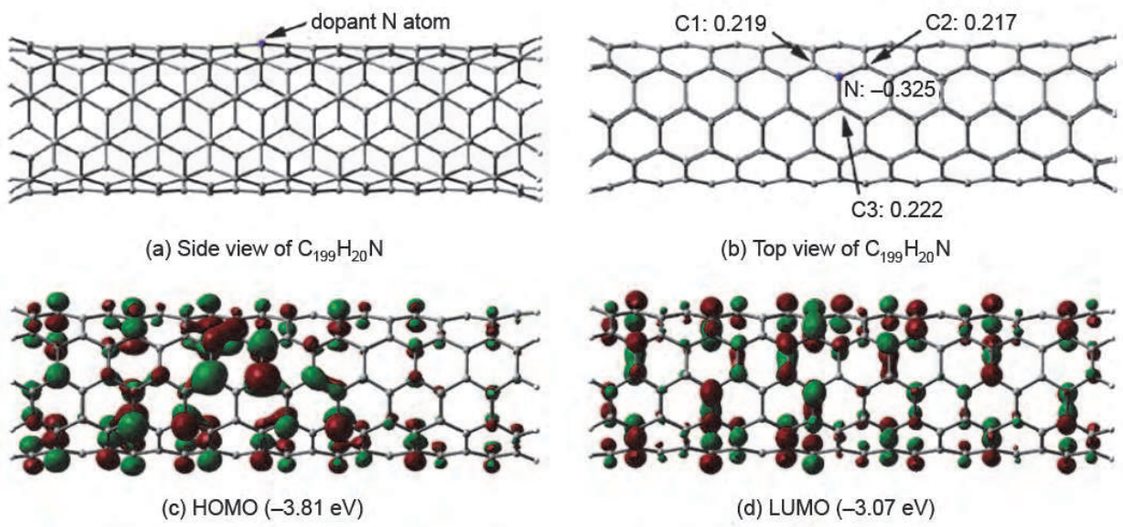

Fig. 3.5. Optimized geometry and FMOs of $C_{199}H_{20}N$. Orbital energies are in parentheses (Liu et al. 2006).

In accord with literature data (Nevidomskyy et al. 2003), the geometry of N-doped HSWCNT model ($C_{199}H_{20}N$) strongly resembles the undoped, defect-free SWCNT ($C_{200}H_{20}$, Figure 3-5). Substitutional doping leads to a decreased HOMO−LUMO gap (0.74 eV) and slight polarization of the nanotube, with the N atom bearing a charge of −0.325.

3.4 Biological applications of defected SWCNTs and reactions with NO: Therapeutics and biosensing

Maintaining homeostasis of physiological NO is critical to biological systems (Miller & Megson 2007). As such, if future nanodevices are implanted into living organisms, it may interact with the biocycles of NO and strongly impact the amount of NO present. Given our studies (Liu et al. 2006), we envision the use of vacancy defective nanotubes in reducing the local concentration of NO by the irreversible chemical reaction depicted in Figure 3-4. For every single vacancy, two molecules of NO are consumed, producing a N-doped SWCNT and one molecule of NO_2 as a byproduct. This process can be controlled in both location and defect concentration by inducing the selective formation of single vacancies by applying external stimuli to the area of interest. We can imagine, for example, the employment of ultraviolet light as a form of medical treatment. This strategy would provide a platform for physicians to carefully control the amount of NO present in any given biological system. Manipulating the local concentration of NO would be achieved by a hybrid approach involving chemically designed pharmaceutical agents such as glyceryl trinitrate and sodium nitroprusside (Figure 3-6), as well as new technologies involving materials such as zeolites (Wheatley et al. 2006) and Pt nanoparticles (Caruso et al. 2007). Recent work on the antithrombotic activity of NO drugs has confirmed that controlled release is essential to these types of treatments and we expect CNTs to play a critical role in the development of new therapeutic techniques in the future.

We can also imagine a scenario in which nanotubes are used as a preventative measure to control the amount of ROS present in the body; in other words, CNTs could act as an artificial antioxidant. Because it is known that the introduction of N atoms into nanotube sidewalls increases clearance rates (Singh et al. 2006), their removal from the biological system may be possible following irreversible NO capture. This suggests that the antioxidant properties of these carbon macromolecules may reverse the damage caused by high-energy processes, including harmful UV-A and UV-B rays from the sun. If defect-free, pristine SWCNTs can be implanted into the human body, environmental stresses may trigger the formation of defects, leading to a decrease in the amount of free biological NO.

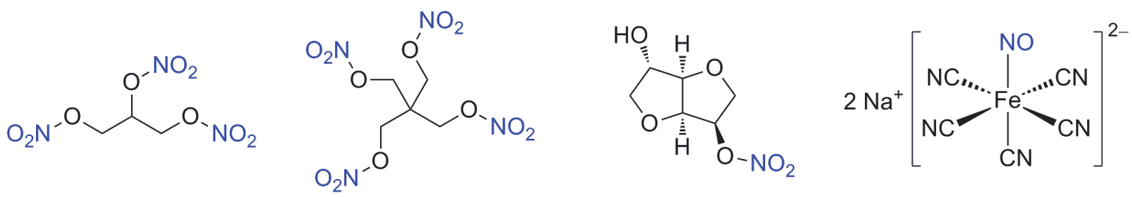

Fig. 3.6. Clinically used NO donor drugs (Miller & Megson 2007).

Defected SWCNTs, if embedded in physiological systems, can serve as a sensor for biological NO. Unlike conventional methods, which involve breath analysis (Menzel et al. 2001), the use of these nanomaterials offers a direct evaluation of NO concentrations at any given location based on the known ability of environmental stresses to induce vacancy defect formation. Quantitative analysis may be achieved via isolation of excreted N-doped SWCNTs in comparison to pristine SWCNTs assuming equal clearance rates. Additionally, we expect that substitutional N-doping results in increased conductivity, since our studies have revealed a decreased HOMO−LUMO gap from 1.38 to 0.74 eV (Liu et al. 2006). If we can monitor electrical current passing through the nanotube, we would have an *in vivo* technique of determining physiological NO. Although the specific details are yet to be determined, it may be possible to orient a nanotube across a lipid bilayer (such as a cell membrane) by capping the ends with hydrophilic ends and subsequently measure its resistance. Alternatively, voltage-sensitive or potentiometric dyes (which change spectral properties in response to voltage changes) may offer another method for non-intrusive analysis (Grinvald & Hildesheim 2004).

As promising as they are, therapeutic applications of SWCNTs necessitate an understanding of nanotoxicology (Oberdorster et al. 2007; Buzea et al. 2007; Lam et al. 2006; Karakoti et al. 2006; Nel et al. 2006). Because macromolecules resist metabolism by macrophages, nanotubes are postulated to persist indefinitely in biological systems, a cause for concern due to bioaccumulation. These effects are further complicated by subtle differences between methods of preparation and the types of defects present that strongly affect intertube interactions and bundle formation. Functionalization is also critical. The introduction of carbonyl (C=O), carboxyl (COOH), and hydroxyl (OH) groups, for example, has resulted in increased cytotoxicity either after contact with cell membranes or following internalization. On the other

hand, functionalization with ammonium cations has demonstrated enhanced clearance rates of these nanomaterials (Singh et al. 2006). Nanotoxicity is proposed to be a result of oxidative stress caused by the generation of ROS in which light-induced formation of electron-hole pairs and unpaired electrons triggers oxidation of molecular oxygen (O_2) to superoxide (O_2^-), promoted by the presence of reactive groups and defects (Karakoti et al. 2006; Nel et al. 2006). Although nature counteracts the effect of ROS, such as by superoxide dismutase or glutathione, accumulation of these reactive species remains problematic. CNTs exhibit a known cytotoxicity in human skin fibroblasts, macrophages, and developing zebrafish embryos, and the particulate nature of these nanomaterials can cause interstitial fibrosis and pulmonary toxicity. Clinically relevant data, however, remains sparse, and recent research has suggested that nanotubes can persist without causing toxicity (Schipper et al. 2008) or any immunological or inflammation reactions (Chiaretti et al. 2008). It is clear that further work is necessary before any clear conclusions can be made regarding nanotoxicology and its impact on human health.

3.5 Substitutional O-doping of SWCNTs via reaction with O_3

In analogy to NO, 5-1DB defects react exothermically with O_3 (Liu et al. 2006a). In traditional organic chemistry, O_3 is a strong oxidizing agent that is capable of cleaving C=C double bonds, generating two C=O bonds via the Criegee mechanism (Kuczkowski 1992). Because the sidewalls of CNTs exhibit π-frameworks of C atoms, it is reasonable to presume that ozonization can take place. We considered a $C_{120}H_{20}$ segment of the (5,5) armchair SWCNT and its defected analog $C_{119}H_{20}$ by removal of a single C atom in the middle of the nanotube. C1 was confirmed as the active C atom within the 5-1DB defect, analogous to our earlier work (Liu et al. 2006).

Only the nine C atoms surrounding the vacancy defect were evaluated in this SWCNT ozonization reaction. Although these C atoms exhibit partial C=C double bond character within the backbone of the defect, the pathway that is most energetically favored involves the direct interaction between ozone and C1 (Figure 3-7). The first step is physisorption of O_3 onto the surface of the SWCNT, forming **INT**, resulting in a transfer of 0.19 electrons from the carbon backbone to O_3. A concerted oxygenation and loss of singlet dioxygen liberates **Product** ($C_{119}H_{20}O$) via a four-membered transition state **TS**. This step is barrierless (−0.3 kcal/mol) and produces a substitutionally O-doped SWCNT with the release of 88.7 kcal/mol. Subsequent relaxation of singlet to triplet O_2 results in further stabilization. We also performed ADMP-AIMD dynamics simulations to confirm our static analysis of the 5-1DB defect ozonization and found that at 300 K, a spontaneous reaction occurs between O_3 and C1 in less than 50 fs. The structure of this O-doped SWCNT differs from our N-doped SWCNT derived from NO (*vide supra*). This is because the bond between C1 and O1 is very strong and exhibits significant double bond character. Hence, it may be more accurate to describe this reaction as a net oxidation of C1 to a ketone. No significant interaction could be observed between C5 and O1.

Because of the ease of oxygenation by ozonization of 5-1DB defects, it has been proposed that such single vacancies are often short-lived species that may rapidly travel through the backbone and annihilate each other (Collins 2010). It would be interesting to see whether other weaker oxygen sources including O_2 and H_2O may be able to oxidize a 5-1DB defect. By studying these processes, we would come to a better understanding of the fate of defect-free and defected SWCNTs within biological systems.

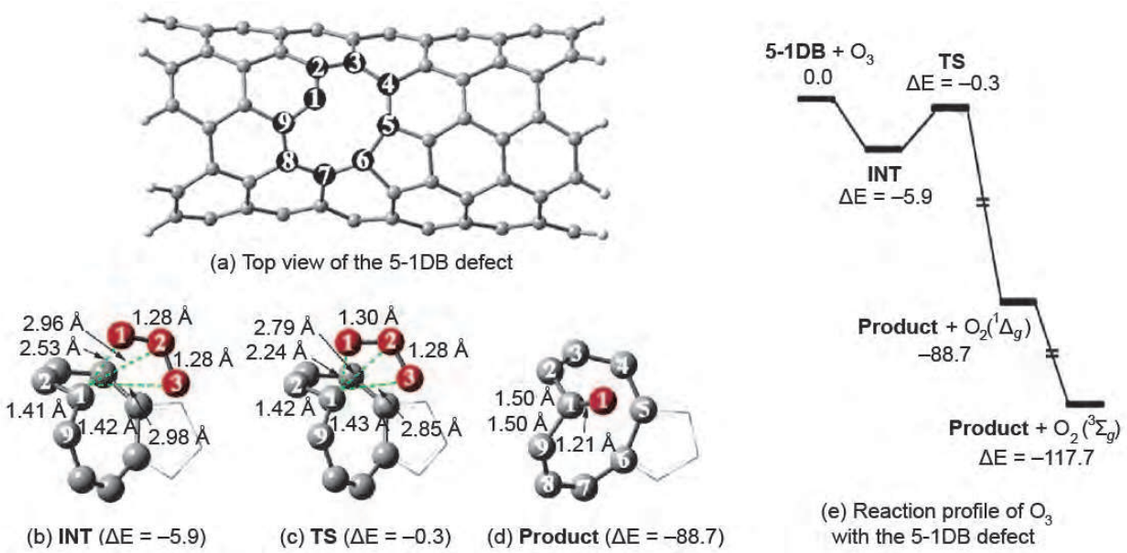

Fig. 3.7. Optimized geometries and energy profiles (with energies in kcal/mol) for the reaction of the defected SWCNT with O_3 (Liu et al. 2006a). Legend: dark grey = C, light grey = H, red = O.

4. Substitutionally doped SWCNTs

4.1 Transition metal-doped SWCNT rods with hydrogen caps

Substitutional doping of SWCNTs with transition metals is yet to be experimentally realized. However, we became particularly interested in this material from theoretical perspective, particularly because of its tremendous potential in nanosensory technology and nanocatalysis based on the rich chemical reactivity of transition metals.

Our studies with N- and O-doped SWCNTs suggest that heteroatoms typically prefer to be situated to the exterior of the nanotube superstructure in which the dopant forms a tripodal structure with the three adjacent C atoms (Liu et al. 2006; Liu et al. 2006a). To confirm this assessment, we used a truncated (5,5) SWCNT capped with H atoms and substituted a single C atom in the middle of the segment with a transition metal considering both the possibility of external doping and internal doping (Chen et al. 2011). Our calculations are consistent with the proposal that *exo* substitution is energetically more favored than the corresponding *endo* HSWCNTs by approximately 2 eV due to an unfavorable interaction between the dopant and the nanotube sidewall, in addition to a slight geometric deformation (Figure 4-1). Overall, the introduction of these heteroatoms does not significantly elongate the nanotube along the longitudinal direction. The net charge distribution in a transition metal-doped SWCNT is mostly localized within the adjacent layers of C atoms surrounding the substitutional dopant, but spin density in open-shell systems can be significantly delocalized. From left to right across the transition metal series, the HOMO (or SOMO for open-shell systems) energy decreases. Thus, transition metal-doped SWCNTs become less reactive toward incoming electrophiles. Within group 10 metals (i.e., Ni, Pd, Pt), the difference in energies between *exo* and *endo* substitutions are larger, which is not unexpected since larger atomic radii will induce more structural strain.

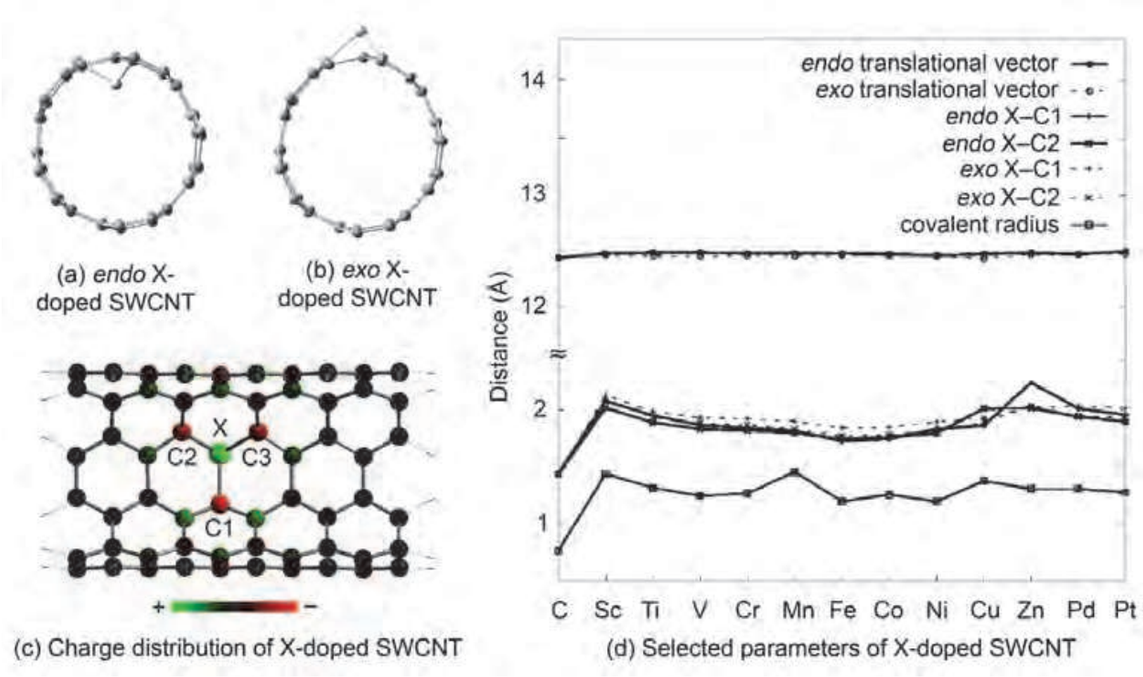

Fig. 4.1. *Endo* and *exo*-substituted transition metal-doped SWCNTs.

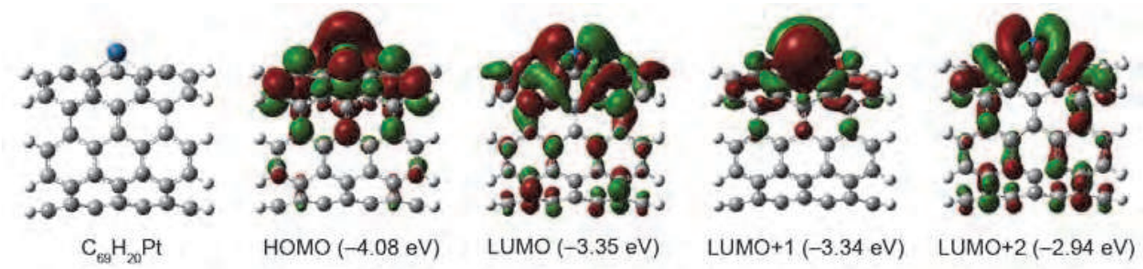

Fig. 4.2. Optimized geometry of $C_{69}H_{20}Pt$ and relevant FMOs. Orbital energies are in parentheses (Yeung et al. 2007). Legend: dark grey = C, light grey = H, blue = Pt.

4.2 Pt-doped SWCNT rods with hydrogen caps

A smaller segment of the (5,5) SWCNT with H caps revealed results consistent with the structure and electronic properties of the larger model described above (Figure 4-2, Yeung et al. 2007). A brief comparison of the FMOs of both models confirms that the shorter $C_{69}H_{20}Pt$ segment suitably describes sidewall doping with the transition metal without the need to use periodic boundary conditions. The dopant Pt atom prefers to adopt a structural arrangement in which it protrudes to the exterior of the sidewall of the SWCNT, due to the larger atomic radius of the Pt atom and subtle interactions between metal *d*-orbitals and the C delocalized π-orbitals. The HOMO−LUMO gap, however, increased to 0.74 eV. In this model, a positive charge of 0.83 resides on the Pt atom in the optimized structure.

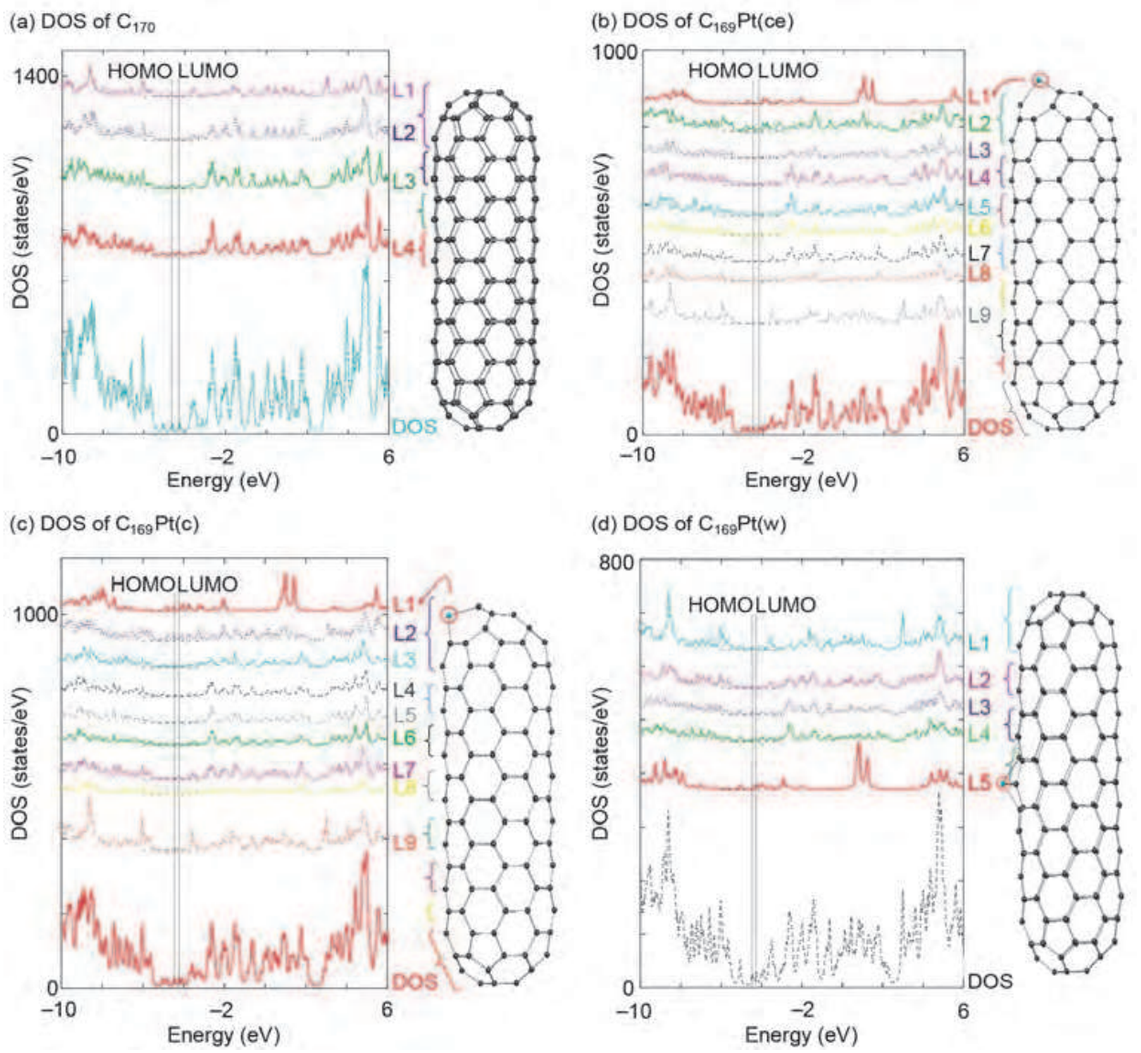

Fig. 4.3. Optimized geometries, DOS, and LDOS of (a) C_{170} with D_{5h} symmetry (ε_{HOMO} = −4.61 eV, ε_{LUMO} = −4.26 eV), (b) $C_{169}Pt(ce)$ with C_s symmetry (ε_{HOMO} = −4.51 eV, ε_{LUMO} = −4.21 eV), (c) $C_{169}Pt(c)$ with C_s symmetry (ε_{HOMO} = −4.48 eV, ε_{LUMO} = −4.25 eV), and (d) $C_{169}Pt(w)$ with C_s symmetry (ε_{HOMO} = −4.46 eV, ε_{LUMO} = −4.26 eV). L1−L9 are the LDOS for each specified layer of atoms as marked on the diagram (Tian et al. 2006).

4.3 Pt-doped SWCNT rods with fullerene caps

Next, we constructed a (5,5) SWCNT rod capped with fullerene hemispheres (C_{170}, Figure 4-3a) and substituted a single C atom with a Pt atom at the cap-end ($C_{169}Pt(ce)$, Figure 4-3b), at the cap ($C_{169}Pt(c)$, Figure 4-3c), and along the sidewall ($C_{169}Pt(w)$, Figure 4-3d, Tian et al. 2006). These nanorods exhibit slightly decreased HOMO−LUMO gaps in comparison to the pristine all-carbon compound.

Pt substitution at the cap-end is the most stable type of doping, with cap-doping and wall-doping sitting 0.8 and 17.9 kcal/mol higher in energy. In our analysis, the triplet spin state was higher in energy than the singlet state. By calculating the FMOs of these model systems (Figure 4-4), we observed a strong interaction between the Pt 5*d* atomic orbitals and the

extended π-framework of the SWCNT backbone, with the greatest effect observed in $C_{169}Pt(w)$. This is because of the better overlap of orbitals where the Pt substitution occurs with roughly mirror-plane symmetry, a feature that is not true for either the cap-end or cap Pt-doped macromolecule.

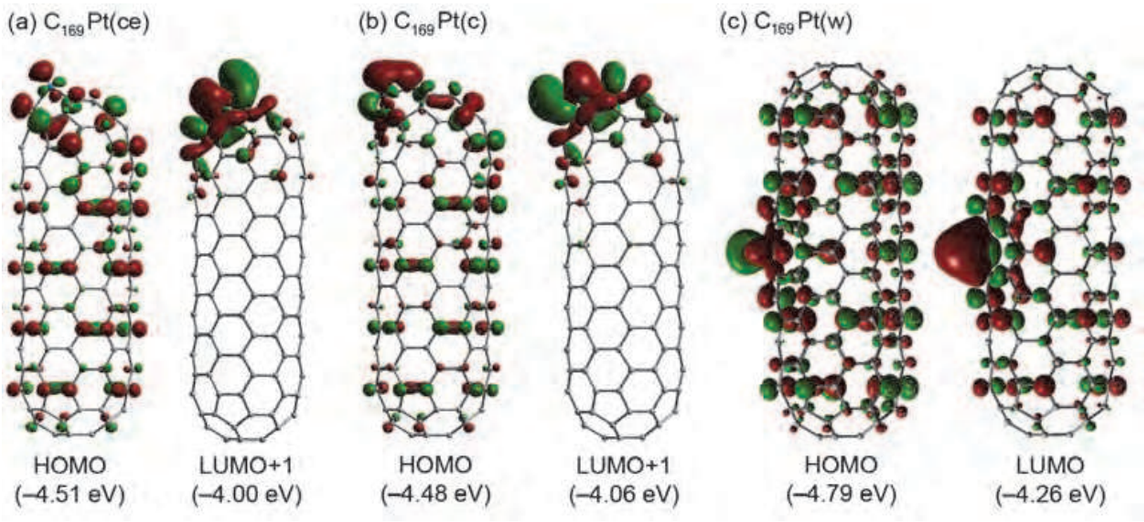

Fig. 4.4. Relevant FMOs for $C_{169}Pt(ce)$, $C_{169}Pt(c)$, and $C_{169}Pt(w)$. Orbital energies are in parentheses (Tian et al. 2006).

4.4 Pt-doped BNNT rods with hydrogen caps

Boron nitride nanotubes are isoelectronic with carbon nanotubes that exhibit different structural, electronic, and chemical features (Wang et al. 2010, Golberg et al. 2010). Indeed, the B−N couple is isoelectronic with the C−C bond but locally exhibits charge separation due to the difference in electronegativity. While B has an empty *p*-orbital and is a coordinatively unsaturated trigonal plane, N has a full octet with an non-bonding pair of electrons in a filled *p*-orbital. Molecular borazine ($B_3N_3H_6$), for example, is an aromatic compound that is isoelectronic and isostructural to benzene (C_6H_6) but is more susceptible to nucleophilic and electrophilic reactions than the all-carbon analog. Hexagonal boron nitride (hBN) is analogous to graphite but displays mechanical hardness and chemical inertness, while graphite is used as a lubricant. In nanotubes, zigzag BNNTs exhibit a non-zero dipole moment because of alternating layers of B and N atoms with band gaps and electronic structures relatively invariant to changes in nanotube diameter and chirality. Importantly, because BNNTs are incombustible at high temperatures and chemically inert, these macromolecules are promising in nanoelectronics.

Natural defects in boron nanotubes can be induced from mechanical fractures, with SW defects consisting of a 5775 structure being more stable than corresponding quadrilateral-octagonal-octagonal-quadrilateral (4884) structure (Karousis 2010). Using a truncated (5,5) BNNT model capped with H atoms ($B_{45}N_{45}H_{20}$, Figure 4-5, Chen et al. 2010), we considered two SW defective structures resulting from a slant B−N bond rotation (SW1) or a vertical B−N bond rotation (SW2). In our defect-free BNNT model, the HOMO−LUMO gap is 6.02 eV, rendering this molecule a good insulator. By introducing SW defects, a decrease in the HOMO−LUMO gap was observed (4.98 and 5.19 eV for SW1 and SW2, respectively).

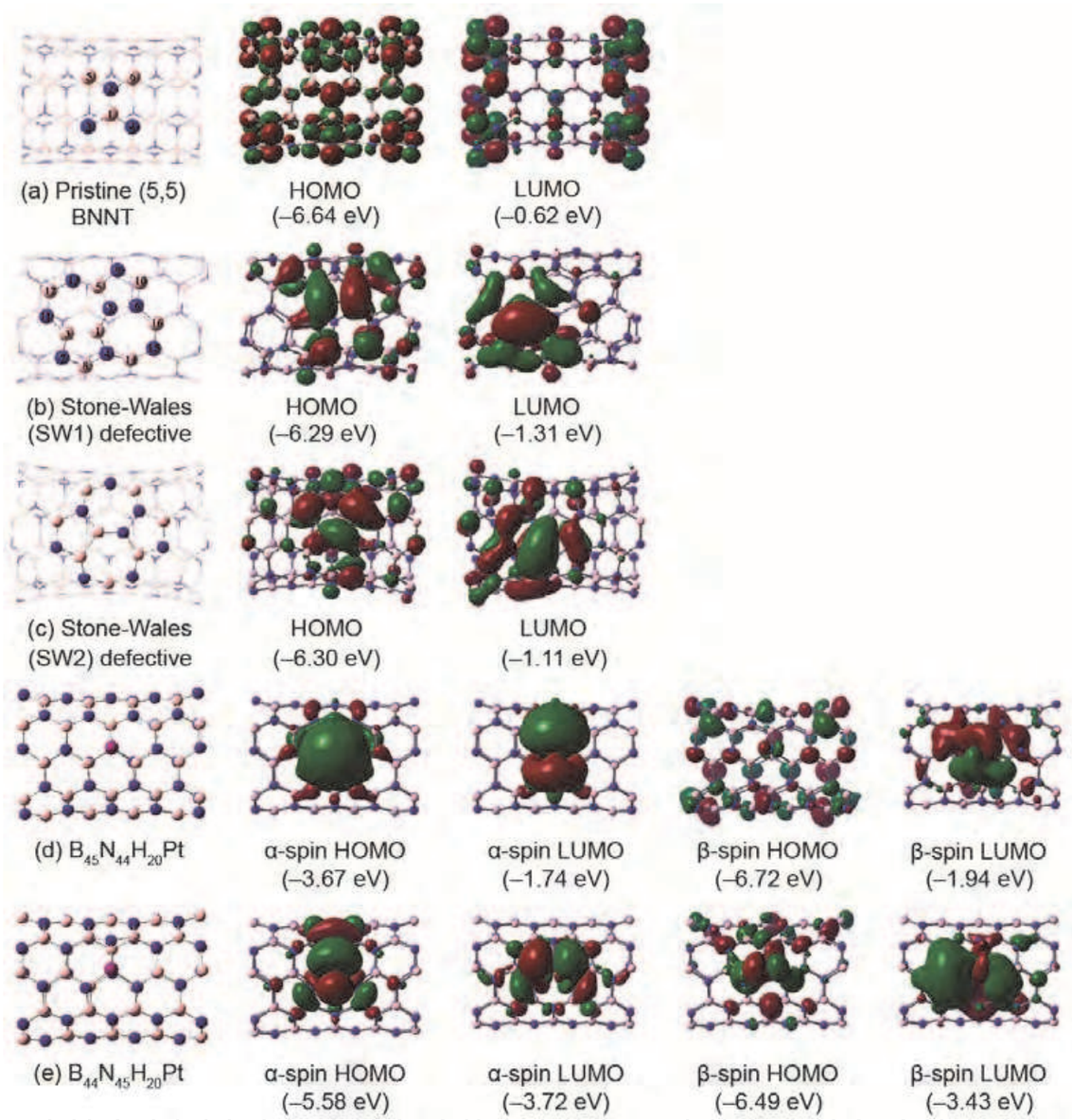

Fig. 4.5. Optimized geometries of (a) a pristine BNNT, (b) a SW1-defective BNNT, (c) a SW2-defective, (d) a Pt-doped BNNT resulting from N-substitution ($B_{45}N_{44}H_{20}Pt$), and (e) a Pt-doped BNNT resulting from B-substitution ($B_{44}N_{45}H_{20}Pt$) and their relevant FMOs (Chen et al. 2010). Orbital energies are in parentheses. Legend: pink = B, navy blue = N, dark pink = Pt.

Vacancy defects in CNTs have been shown to undergo incorporation of transition metal atoms into their backbone (Yang et al. 2006; Zhuang et al. 2008). Substitutional doping of BNNTs is a logical extension, although replacement of either a single N or B atom yields two different materials (Figure 4-5). Although the mechanism of Pt doping is unclear, our studies confirm the existence of doublet ground states and a decreased band gap in these nanomaterials (Chen et al. 2010). Pt-doped BNNTs, unlike pristine and SW-defective BNNTs, are semiconducting.

4.5 Adsorption of gases onto Pt-doped SWCNTs

Discrete organometallic Pt complexes and metal surfaces alike can undergo coordination or adsorption to gas molecules. Hence, we expect similar reactivity with Pt atoms embedded within the sidewall of a carbon nanotube (Yeung et al. 2010).

Carbon monoxide is an important ligand for organometallic complexes and has demonstrated the ability to undergo physisorption onto metal surfaces (Orita et al. 2004). Although the C≡O triple bond of CO is polarized with a reactive lone-pair of electrons on the C, we imagined that adsorption would be possible via either C-end adsorption (a **C**O-adsorbed HSWCNT) or O-end adsorption (an **O**C-adsorbed HSWCNT, Figure 4-6). Both processes were found to be exothermic, with C-end adsorption liberating 41.2 kcal/mol while O-end adsorption only produced 7.0 kcal/mol (Table 4-1). This coordination is a coordinate dative bond, in which the C atom donates its pair of electrons into a metal *d*-orbital, causing a backdonation of electrons to the π^*-orbital of the adsorbate. The result is a lengthening the C≡O triple bond. Indeed, we observe a slight elongation in the adsorbed CO molecule for **C**O-adsorption, from 1.18 Å in the free gas to 1.19 Å, and a net charge of −0.12 on the adsorbate. The bond length between the Pt atom and the CO molecule was 1.97 Å. In contrast, **O**C-adsorption did not display the same type of bond stretching and was a weaker interaction overall.

Since Pt complexes commonly hosts six ligands in its coordination sphere, we explored the possibility of multiple adsorption. We successfully identified a structure in which two CO molecules underwent coordination to the Pt center through C-end adsorption (Figure 4-6). The $(\mathbf{C}O)_2$-adsorbed HSWCNT was formed with a further release of energy (36.8 kcal/mol per CO molecule) and displayed almost identical orientation of both adsorbates. The second adsorption triggered an increase in distance between the Pt atom and the adsorbate to 2.00 Å, while the net charges on each CO molecule decreased to −0.05. Attempts to probe the possibility of triple adsorption did not afford structures in which the CO molecules were bound strongly to the Pt atom via C-end adsorption; instead, a third additional molecule of CO displayed a weak interaction with the nanotube sidewall. This process is uphill in energy from the doubly-adsorbed intermediate. Clearly, the steric bulk of the nanotube precludes the possibility of triple adsorption.

Nitrogen monoxide is not commonly encountered in coordination chemistry, unlike its related charged cousins NO^+ and NO^-, but are known to interact with Pt surfaces (Backus et al. 2004). In analogy to CO-adsorption, coordination between the Pt atom and the adsorbate can take place via N-end adsorption or O-end adsorption. Our calculations revealed that **N**O-adsorption is energetically preferential to **O**N-adsorption (Figure 4-6). In all geometries examined, the quartet spin state exhibited higher energy than doublet states (which can arise from either singlet or triplet Pt-doped SWCNT starting materials). The adsorption of NO onto the Pt atom embedded in the nanotube results in a complex bearing a charge of 0.99 on the Pt center and an increased HOMO−LUMO gap to 0.84 eV. Multiple adsorption was observed to occur in an unsymmetrical fashion in which one of the O atoms of the adsorbate molecules points away from the surface of the nanotube sidewall. This process is less exothermic than single adsorption, and consequently, simultaneous coordination of three molecules of NO was not considered.

Ammonia is a common N-containing ligand for Pt complexes, including the famous chemotherapy drug cisplatin, $PtCl_2(NH_3)_2$ (Boulikas & Vougiouka 2003). Heterogeneous Pt surfaces are critical to NH_3 chemistry, such as in the industrial oxidation of NH_3 to NO in nitric acid production. Unlike CO and NO, however, NH_3 does not exhibit a low-lying π^*-orbital to allow backbonding to occur. In our studies, the adsorption energy between NH_3

and the Pt-doped SWCNT was –31.8 kcal/mol and the resulting **N**H_3-adsorbed HSWCNT exhibited a HOMO−LUMO gap of 0.73 eV and a Pt–N bond distance of 2.25 Å (Figure 4-6, Yeung et al. 2008). Biadsorption of NH_3 occurred with 57.1 kcal/mol release of energy (28.5 kcal/mol per NH_3 molecule).

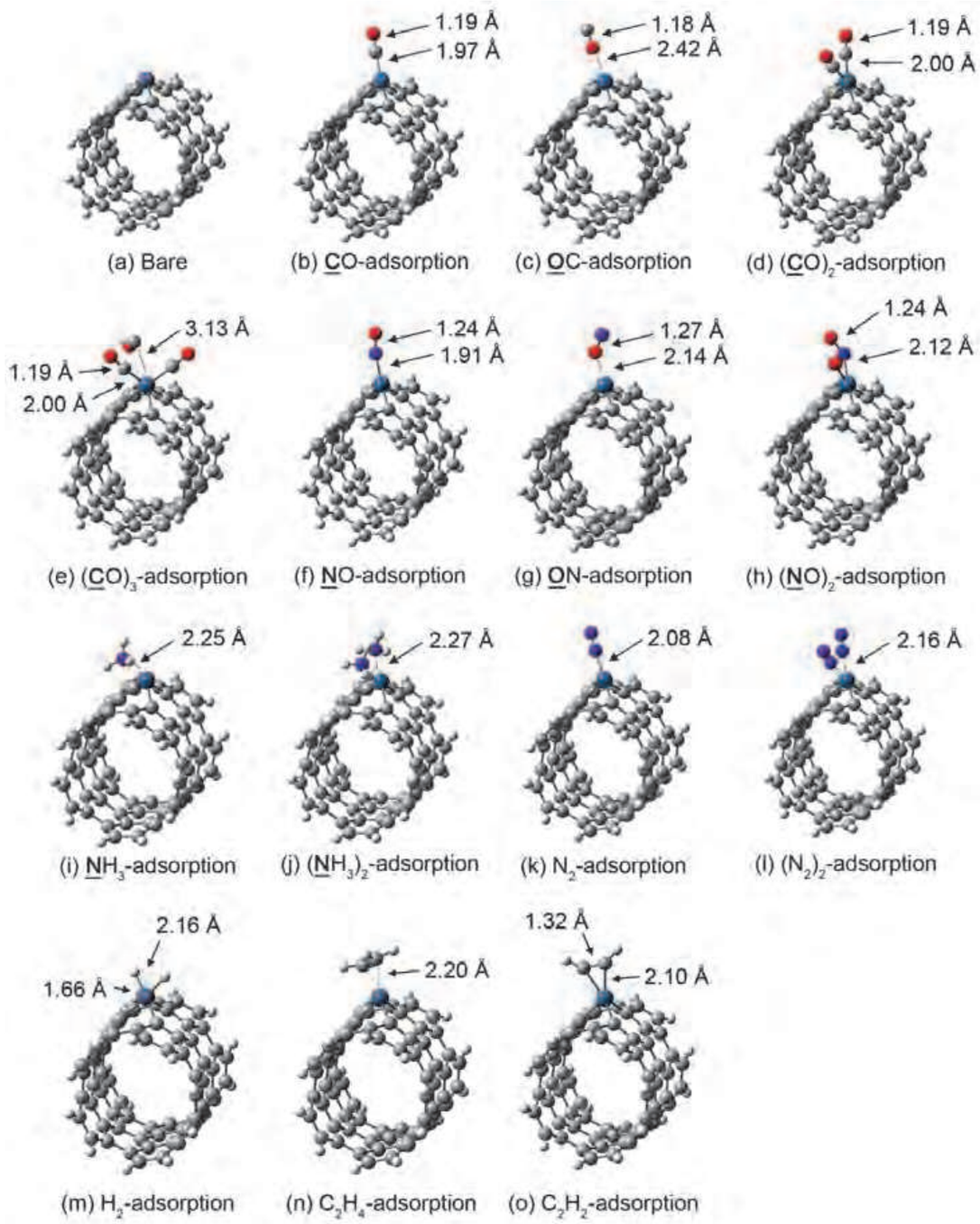

Fig. 4.6. Optimized geometries for gas-adsorbed HSWCNTs (Yeung et al. 2010). Legend: dark grey = C, light grey = H, navy blue = N, red = O, blue = Pt.

Adsorbate	Spin state	ΔE[a]	*d*(PtX)[b]	*d*(XY)[c]	*q*(Pt)[d]	*q*(XY)[e]	*q*(C)[f]
None	Singlet	0	N/A	N/A	0.82	N/A	−0.41
	Triplet	0	N/A	N/A	0.84	N/A	−0.49
CO[g]	Singlet	−41.2	1.97	1.19	0.85	−0.12	−0.43
	Triplet	−33.1	1.96	1.20	0.83	−0.15	−0.46
OC[g]	Singlet	−7.0	2.42	1.18	0.87	−0.02	−0.41
	Triplet	−6.8	2.35	1.19	0.88	−0.06	−0.45
(**C**O)$_2$[g]	Singlet	−73.7	2.00, 2.00	1.19, 1.19	0.83	−0.05, −0.05	−0.49
	Triplet	−59.0	2.00, 2.00	1.19, 1.19	0.78	−0.02, −0.02	−0.49
(**C**O)$_3$[g]	Singlet	−71.4	1.98, 2.00, 3.13	1.19, 1.19, 1.19	0.77	0.01, −0.01, −0.06	−0.37
	Triplet	−73.7	2.03, 2.03, 2.41	1.18, 1.18, 1.19	0.76	0.05, 0.05, −0.13	−0.46
NO[g]	Doublet	−47.0 (−56.5)[h]	1.91	1.24	0.99	−0.39	−0.39
	Quartet	−46.2	2.00	1.25	0.95	−0.38	−0.34
ON[g]	Doublet	−23.2 (−32.7)[h]	2.14	1.27	0.98	−0.37	−0.34
	Quartet	−30.0	2.12	1.29	1.00	−0.44	−0.33
(**N**O)$_2$[g]	Singlet	−69.9	2.10, 2.12	1.24, 1.24	0.99	−0.24, −0.28	−0.36
	Triplet	−77.8	2.12, 2.12	1.24, 1.24	0.99	−0.25, −0.25	−0.35
NH$_3$[i]	Singlet	−31.8	2.25	N/A	0.88	0.18	−0.44
	Triplet	−31.3	2.23	N/A	0.87	0.18	−0.50
(**N**H$_3$)$_2$[i]	Singlet	−57.1	2.27, 2.27	N/A	0.92	0.18, 0.18	−0.48
	Triplet	−55.3	2.26, 2.26	N/A	0.86	0.19, 0.19	−0.49
N_2	Singlet	−24.7	2.08	1.16	0.91	−0.14	−0.41
	Triplet	−25.9	2.05	1.16	0.91	−0.18	−0.44
$(N_2)_2$[i]	Singlet	−43.9	2.16, 2.16	1.16, 1.16	0.93	−0.09, −0.09	−0.42
	Triplet	−41.7	2.16, 2.16	1.16, 1.16	0.89	−0.09, −0.09	−0.41
H_2[j]	Singlet	−11.3	1.66, 1.68[k]	2.16	0.77	−0.34	−0.33
	Triplet	−6.0	1.66, 1.66[k]	2.19	0.74	−0.34	−0.43
C_2H_4[j]	Singlet	−26.4	2.31, 2.20[k]	1.43	0.95	−0.25	−0.35
	Triplet	−24.7	2.31, 2.30[k]	1.42	0.92	−0.16	−0.37
C_2H_2[j]	Singlet	−31.4	2.13, 2.10[k]	1.32	0.98	−0.38	−0.34
	Triplet	−25.3	2.17, 2.15[k]	1.30	0.92	−0.27	−0.31

[a]Total stabilization energy (in kcal/mol).
[b]Distance (in Å) between Pt and X of XY.
[c]Distance (in Å) between X and Y of XY.
[d]Partial charge on Pt.
[e]Net partial charge on XY.
[f]Net partial charge on the C atoms of the SWCNT adjacent to Pt.
[g](**X**Y)$_n$ refers to an *n* X-end adsorbed HSWCNT fragment.
[h]Total stabilization energy (in kcal/mol) from triplet ground state bare Pt-doped SWCNT in parentheses.
[i]End-on adsorption.
[j]X = Y. These adsorbates are bound in a side-on fashion.
[k]Distance (in Å) between Pt and both X in X_2.

Table 4.1. Binding energy and geometrical data for nanotube-adsorbate complexes $C_{69}H_{20}Pt(XY)$ (Yeung et al. 2007; Yeung et al. 2010).

Nitrogen gas is distinct from the aforementioned adsorbates because of its lack of inherent polarity. If our Pt-doped nanotubes will be applied as nanosensors, the ability to detect simple and unpolarized small molecules is critical. The interaction between N_2 and Pt

surfaces is important to the industrial fixation of nitrogen via the Haber-Bosch process. In transition metal complexes, N_2 can coordinate with either an end-on orientation (with the N atom acting as a σ-donor) or a side-on orientation (with the N≡N triple bond acting as a π-donor). We found that Pt-doped SWCNTs prefer to bind N_2 with end-on geometry, as both end-on and side-on binding converged to give the same structure (Figure 4-6). The energy released was significantly less than CO adsorption (24.7 kcal/mol), because the electrostatic interactions between an unpolarized adsorbate such as N_2 and the HSWCNT is weak. The observed N≡N bond distance was lengthened slightly from 1.15 Å in the free gas to 1.16 Å in this complex and the net charge on the adsorbate was −0.14, signifying a net donation of electrons from the Pt atom to the ligand. The calculated HOMO−LUMO gap was 0.81 eV. We also identified a doubly adsorbed complex in which two molecules of N_2 bound to the Pt atom via end-on coordination. The energy released per molecule was 22.0 kcal/mol, close to that of single adsorption, possibly because the weaker interaction between the Pt and the adsorbate minimizes steric repulsion between the two coordinated N_2 molecules.

Hydrogen gas is the lightest diatomic molecule. Activation of H_2 with Pt has found tremendous application in organic synthesis in the catalytic hydrogenation of alkenes and alkynes. Since our Pt-doped SWCNT has the capability of binding linear diatomic molecules, we reasoned that either H_2 physisorption or chemisorption is possible. With our (5,5) $C_{69}H_{20}Pt$ nanotube model, we obtained a geometry in which H–H bond cleavage occurred. In fact, a distance of 2.16 Å was observed between the two H atoms. The energetic preference for this reaction was −11.32 kcal/mol. In the optimized structure, the HOMO−LUMO gap was 0.70 eV, and a charge of 0.77 was present on the Pt atom, while 0.34 had transferred to the chemisorbed H_2. (For other studies of H_2 adsorption, see section 4.7.)

Carbon-carbon multiple bonds are excellent substrates for coordination to transition metals. In particular, the adsorption of C=C and C≡C bonds to Pt surfaces is an important process to catalytic hydrogenation reactions. To this end, we considered the adsorption of the simplest two-carbon alkene ethylene (C_2H_4) onto the (5,5) Pt-doped SWCNT model and found that 26.4 kcal/mol were released upon physisorption. The HOMO−LUMO gap increased to 0.88 eV in this case and the observed C=C bond distance was 1.43 Å. A net negative charge of –0.25 on the adsorbate was determined. When we optimized structures involving the simplest two-carbon alkyne acetylene (C_2H_2), we observed a strong interaction between the adsorbate and the HSWCNT. Alkynes are known to interact with transition metals through weak donation of π-electrons of the adsorbate to the metal and in some circumstances can result in oxidative addition, generating a metallocyclopropene complex. In our studies, C_2H_2 coordination liberated 31.4 kcal/mol and resulted in a significant lengthening of the C≡C bond distance from 1.23 Å in the free gas to 1.32 Å. Additionally, the terminal C–H bonds are no longer co-linear with the C≡C bond but instead are bent. The HOMO−LUMO gap roughly paralleled that of C_2H_4 adsorption (0.88 eV), and a net charge of −0.38 was detected on the alkyne. The Pt center was found to bear a charge of 0.98 and the separation between the Pt atom and either C atom of C_2H_2 was approximately 2.15 Å. Hence, the interaction between C_2H_2 and CNTs substitutionally doped with Pt is indeed chemisorptive in nature and yields a metallocyclopropene. In other words, C_2H_2 adsorption induces a rehybridization of the C atoms from *sp* to sp^2.

4.6 Applications of Pt-doped SWCNTs: Chemical sensors and nanoelectronics

Because of the ability for Pt-doped SWCNTs to adsorb different gases, it is reasonable to consider using these nanomaterials as chemical sensors. Developing a nanodevice capable of sensing the presence of various analytes depends primarily upon the ability to monitor

minor changes in electronic structure, such as by measuring conductance across a nanowire. Designing new nanosensory technology for molecules including CO, NO, NH_3, and H_2 would be worthwhile (Rouxinol et al. 2010; Wang & Yeow 2009).

The first CNT gas sensor was reported by Kong, in which a semiconducting SWCNT acted as a channel to conduct the source-drain current in a field-effect transistor (FET, Kong et al. 2000). In a typical FET, the SWCNT connects the source and drain, and current is passed by applying an external voltage. The surface of the SWCNT is exposed to the atmosphere, hence allowing detection to take place (Rouxinol et al. 2010; Wang & Yeow 2009). Current is measured as a function of bias voltage (V_B) and gate voltage (V_G).

A variant of this design involves interdigitated electrodes (IDE). In a system developed by Li (Li et al. 2003), a solution casting process was used to prepare a device containing a network or mesh of SWCNTs on a Ti and Au IDE on a layer of silicon dioxide (SiO_2). Drop-deposition of the nanotubes was the method of choice for delivery. This nanosensor combines the advantages of single nanotube transistors and film-based sensors since there is a large density of nanotubes present on the IDE and the array configuration provides excellent electrical contact between the SWCNTs and the electrodes while maintaining good accessibility for gas adsorption.

A complementary strategy known as the resonant-circuit sensor (RCS) method was described by Chopra (Figure 4-7, Chopra et al. 2002). In this scenario, carbon nanotubes are adsorbed onto a Cu resonator and irradiated by a microwave signal from a radio frequency transmitter. As a result of interaction with the sensor resonator, a strong signal is generated at its resonant frequency. Detection of analytes hence depends on measuring the shift of the frequency between the received signal and the transmitted signal.

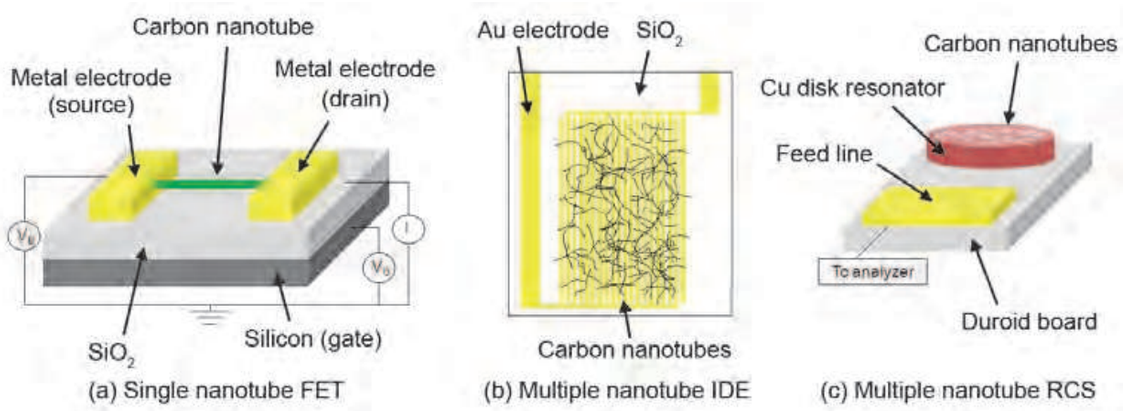

Fig. 4.7. Schematic diagrams for nanotube sensors. (a) A single nanotube field-effect transistor (Rouxinol et al. 2010; Wang & Yeow 2009). V_B = bias voltage, V_G = gate voltage, I = current. (b) A multiple nanotube interdigitated electrode device (Li et al. 2003). (c) A multiple nanotube resonant-circuit sensor (Chopra et al. 2002).

In devices in which measurements of conductivity form the basis of quantitative analysis, minor fluctuations in electronic structure can be evaluated by considering the amount of charge transfer that takes place between the SWCNT and the small molecule adsorbate. Analysis of the HOMO−LUMO gap may also provide some insight. Peng and co-workers have described that charge transfer resulting from adsorption can change conductance along the axis as follows:

$$\Delta Q = C_g \cdot \Delta V_g = \delta\theta \frac{\pi dl}{\sigma} \tag{13}$$

where ΔQ is the charge transfer, C_g is the capacitance, and ΔV_g is the observed voltage change (Peng et al. 2003). The nanotube length and diameter are l and d, respectively, and σ and θ are the molecular cross-section area and coverage, respectively. For the majority of analytes considered (Table 4-2), adsorption results in a net charge transfer from the Pt-doped SWCNT to the gas and an increased HOMO−LUMO gap. This suggests a net decrease in conductivity and a net increase in resistivity.

In our investigations (Yeung et al. 2010), the magnitude of charge transfer between adsorbate and the Pt atom is relatively small. However, it has been demonstrated a change of 0.28 is sufficient for being experimentally measurable. We predict that extending our model Pt-doped SWCNTs in either direction *ad infinitum* should enhance sensitivity enough such that a practically useful device can be prepared using these macromolecules. Cooperativity and synergy between nearby transition metals embedded in the nanotube sidewall is another possible feature that warrants further investigation. Other strategies, such as using polymer matrices to encapsulate our HSWCNTs, may help. In fact, the inclusion of CNTs in insulating polymer matrices can produce a hybrid material that is conductive above a certain filler concentration known as the percolation threshold (Moniruzzaman & Winey 2006). Yodh and co-workers have confirmed that the percolation threshold can be as low as 0.005 vol% in SWCNT/epoxy composites (Bryning et al. 2005). Should an amplification of signal be observed in the CNT/polymer hybrid, selective chemical sensing of individual gas molecules may become possible. The ideal nanosensor would be a small handheld device with short response times, high sensitivities, and the ability to differentiate between analytes. Using Pt-doped SWCNTs is potentially advantageous to undoped CNTs and may revolutionize biomedical, automotive, food, agriculture, and manufacturing industries. Detection techniques of relevance to environmental pollutants and national security will also benefit from these materials.

Analyte	**Charge transfer**[a]	**G_{HL} (eV)**	**ΔG_{HL}**[f] **(eV)**
None	N/A	0.74	0.00
CO[b]	0.05	0.78	0.04
NO[c]	0.28	0.74	0.00
NH_3[d]	−0.18	0.75	0.01
N_2[e]	0.09	0.81	0.07
H_2	0.34	0.70	−0.04
C_2H_4	0.25	0.88	0.14
C_2H_2	0.38	0.88	0.14

[a]Represents charge donated from the Pt-doped SWCNT to the adsorbate.
[b]Represents (**C**O)$_2$-adsorbed HSWCNT.
[c]Represents (**N**O)$_2$-adsorbed HSWCNT.
[d]Represents (**N**H$_3$)$_2$-adsorbed HSWCNT.
[e]Represents (N_2)$_2$-adsorbed HSWCNT.
[f]Represents the change in the HOMO−LUMO gap upon adsorption.

Table 4.2. Average charge transfer and HOMO−LUMO gap (G_{HL}) data for nanotube-adsorbate complexes with side-on binding motif (Yeung et al. 2010).

Other than chemical sensors, Pt-doped SWCNTs may be applied to nanoelectronics. There have already been significant studies involving the utilization of CNTs as FETs, optoelectronic devices, and nanoelectromechanical systems (NEMS, Park 2004; Srivastava et al. 2003; Fuhrer 2003; Tsukagoshi et al. 2002). Technology using CNTs in FETs has already been commercialized (e.g., Infineon Technologies). In this specific FET, which features a back-gate, the CNT is situated at the top of the electrodes, separated from each other by a dielectric spacer to the back-gate. The conductive nanochannel hence provides an electrical connection between the source and drain electrodes and acts as a molecular wire. Applying these devices to more complex components such as nonvolatile molecular memory elements is a rapidly advancing field.

Because Pt-doped SWCNTs undergo conductivity changes when exposed to different types of gases, we envision the design of a new element of control in nanoelectronics in which varying the gas atmosphere will allow control of electrical current. For instance, if the conductance of a CNT nanowire is too high, introducing an atmosphere of CO should provide an immediate increase in resistivity and a decreased current. This effect would be compounded if the nanotube backbone is substitutionally doped at multiple sites. The key advantage to this type of electronic manipulation is the ability to control conductivity and resistivity *in a reversible fashion*. By simply purging the atmosphere with an inert gas, such as argon, any adsorbed molecules that were previously used to modulate electrical current can be removed. Because of the high diffusion rates of gases, extremely fast circuit breaks are possible. In the future, more complicated devices may contain substitutionally doped SWCNTs of different elements. Each CNT nanowire would be affected to a different extent depending on the adsorbate. Such careful control of nanocircuits would provide engineers with new tools for the development of new nanodevices.

4.7 Adsorption of H_2 onto Pt-doped SWCNTs and BNNTs

The incorporation of Pt into the sidewall of CNTs provides a unique chemical reactivity, particularly with small molecules, that is otherwise not possible. In our studies of H_2 adsorption (Yeung et al. 2010), our (5,5) $C_{69}H_{20}Pt$ model revealed a strong interaction between hydrogen and the Pt atom, resulting in a chemisorptive process in which the two H atoms became split. We also pursued investigations of Pt-doped nanorods capped with fullerenes and their ability to perform H–H bond cleavage (Tian et al. 2008). To our surprise, with the larger $C_{169}Pt$ nanorods, both cap-doped HSWCNTs underwent physisorption with H_2, releasing only 2.0 kcal/mol of energy. We were pleased to find, however, that wall-doped nanorods performed a similar chemisorption as predicted by our H-capped model.

The isoelectronic Pt-doped BNNTs was also considered in H_2 adsorption (Li et al. 2009). In their work, up to three equivalents of H_2 can undergo physisorption to the Pt center. This is in stark contrast to our Pt-doped SWCNTs which can perform chemisorption. Clearly, the electronic nature of the carbon backbone plays a role in determining the chemical reactivity of the Pt atom.

4.8 Applications of H_2 adsorption onto Pt-doped SWCNTs and BNNTs: Hydrogen storage and nanocatalytic hydrogenations

The use of CNTs in hydrogen storage remains an active area of research (Yao 2010). For instance, defective CNTs and their ability to undergo adsorption of H_2 has also been investigated (Gayathri et al. 2007). If Pt-doped SWCNTs and Pt-doped BNNTs are to be

used as hydrogen storage materials, then their ability to adsorb H_2 reversibly becomes important. As we have described above, Pt-doped SWCNTs (especially wall-doped) tend to undergo chemisorption with H_2 and release of hydrogen may require external input of energy (Yeung et al. 2010; Tian et al. 2008). On the other hand, a reversible interaction between Pt-doped BNNTs and hydrogen appears to be much more favorable. Careful tuning of the electronic properties of the Pt atom will be necessary to achieve the right balance to provide facile and reversible adsorption and desorption. In an infinitely long SWCNT with numerous Pt dopants, we expect that efficiency will be improved.

Perhaps more interesting than H_2 storage is the ability for Pt to activate H_2. While many transition metals are known to cleave hydrogen homolytically, forming a formal metal dihydride, the substitutional doping strategy that we have described is of particular interest because of potential use of these nanomaterials as catalysts for catalytic hydrogenation. We have already discovered that C=C double bonds (in C_2H_4) bind reversibly to the Pt atom of Pt-doped SWCNTs, while H_2 undergoes complete dissociation. At an appropriate doping concentration and geometry, we envision two Pt atoms working together to perform hydrogenation of alkenes such as ethylene. On the first Pt atom, H_2 would undergo H–H bond breaking via oxidative addition. Simultaneously, on the second Pt atom, one molecule of alkene can bind transiently. Because of the weak interaction, it is reasonable to presume that the alkene can insert into the Pt–H bond and form a new Pt–C bond. Finally, reductive elimination will furnish the reduced alkane product. Should this transformation be possible, it would be a modern variant of Pt metal catalyzed hydrogenation. The only reason that catalytic hydrogenation would become possible using nanotubes is because of the innate chemical reactivity of Pt. Hence, substitutional doping may open the door for examining other types of nanocatalysis, one of which is described below.

4.9 Applications of Pt-doped SWCNTs: Lewis acidity and nanocatalysis

Pt-doped SWCNTs can undergo adsorption with CO (Yeung et al. 2007). Based on this reactivity, we investigated model alkylplatinum complexes through DFT, considering all possible trimethylplatinum species with formulae $PtMe_3(CO)_x^{n+}$ (where x = 0 to 3 and n = –3 to 1, Figure 4-8). Based on the observed geometry and partial charge analysis, we chose $PtMe_3(CO)_x^+$ for comparison purposes. By examining the FMOs of $PtMe_3(CO)_x^+$ and comparing it with the model (5,5) Pt-doped SWCNT, we found remarkable similarities, hence suggesting that the reactivity of the Pt atom as a substitutional dopant should roughly parallel that of $PtMe_3^+$. Interestingly, we observed facile triple adsorption in the case of the monomeric $PtMe_3^+$ complex, while this process was not possible in the HSWCNT. This dichotomy in reactivity can be attributed to the steric bulk of the nanotube sidewall and a decreased electron density in the reactive *d*-orbital of the Pt dopant atom.

$PtMe_3^+$ is a known Lewis acid catalyst (Hsieh et al. 2007; Procelewska et al. 2005). Hence, we considered the use of Pt-doped SWCNTs as nanocatalysts (Yeung et al. 2011). To evaluate Lewis acidity, we first performed vibrational analyses on CO-adsorbed Pt complexes, since the C≡O stretch is an indicator for the level of backdonation from the metal center to the ligand. Next, the nuclear magnetic resonance (NMR) chemical shift (δ) of the olefinic H in the β position of an α,β-unsaturated carbonyl compound, specifically maleic anhydride (MA), was evaluated upon coordination to the Pt atom, a technique first described by Child and co-workers (Childs et al. 1982; Laszlo & Teston 1990). Compared to the uncomplexed MA, Lewis acid coordination should generate a positive downfield shift of the proton

resonance at the β position due to a deshielding effect and consequently, chemical shift difference ($\Delta\delta$) is a direct measure of Lewis acidity. Finally, to truly test our hypothesis of Pt-doped SWCNTs as Lewis acids in nanocatalysis, we envisioned the use of these macromolecules as catalysts for the Diels-Alder reaction between MA and cyclopentadiene (CPD), a [4+2] cycloaddition. This reaction generates two possible products, the *exo* and *endo* adducts. If substitutional doping of Pt into a nanotube sidewall bears some resemblance to $PtMe_3^+$, then catalysis is likely. We were particularly interested to evaluate both rate enhancement and effects on stereoselectivities in this transformation.

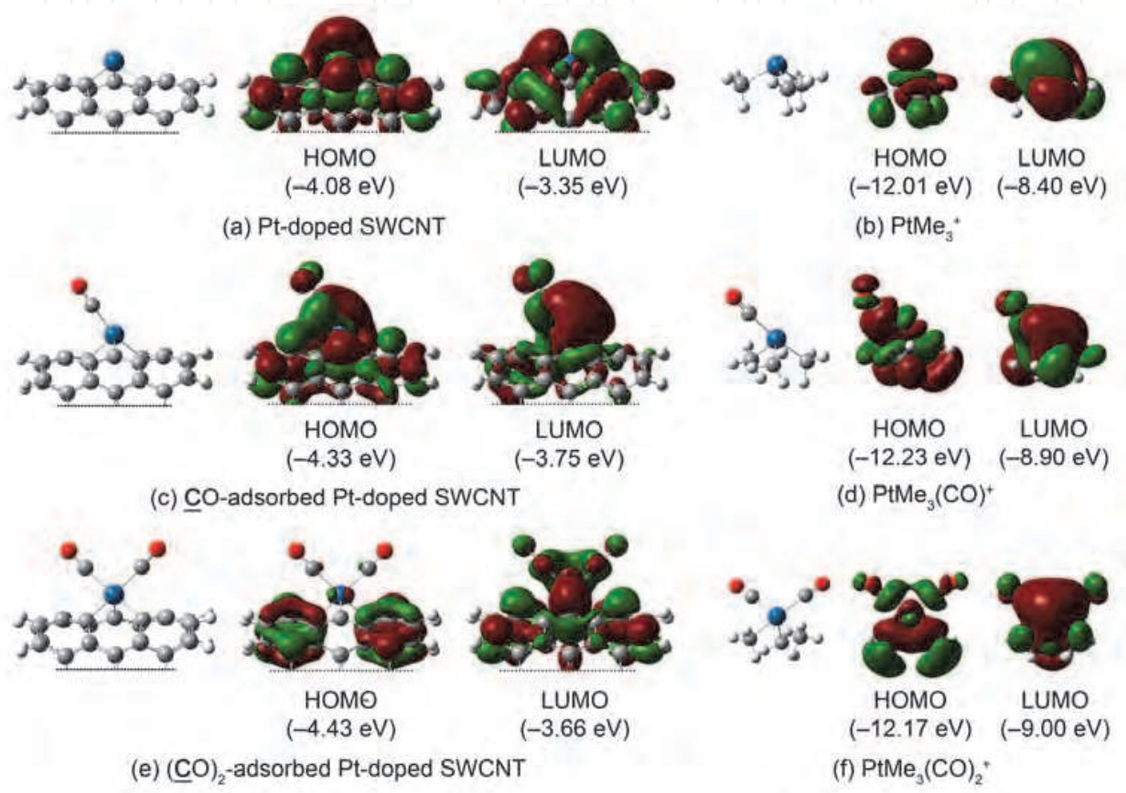

Fig. 4.8. Optimized geometries and FMOs for (5,5) Pt-doped SWCNT and model complex $PtMe_3^+$ (Yeung et al. 2007). Orbital energies are in parentheses.

Other than $PtMe_3^+$, we examined other Pt-based model systems (Figure 4-9) for Pt-doped SWCNTs, including $PtPh_3^+$, Pt-doped phenaline, Pt-doped sumanene, Pt-doped corannulene, and Pt-doped C_{24} fullerene (which exists as one of two isomers, involving either Pt substitution at a pentagon-pentagon-pentagon junction or PPP, or a hexagon-pentagon-pentagon junction or HPP). We were intrigued to additionally evaluate the role of the delocalized π-electrons, particularly as it pertained to curvature (Lu & Chen 2005). Because of computational limitations, we chose a (5,0) Pt-doped SWCNT segment capped with ten H atoms of molecular formula $C_{49}H_{10}Pt$ and calculated a geometry in which the Pt atom protrudes to the exterior of the nanotube sidewall. Of the model complexes considered, only $PtMe_3^+$ and $PtPh_3^+$ displayed less pyramidalization at the Pt atom than the HSWCNT ($\sum$ = 297.5° and 315.4°, respectively, versus $\sum$ = 282.1°). Pt-doped sumanene, corannulene, and C_{24} are all more highly pyramidalized ($\sum$ < 270°).

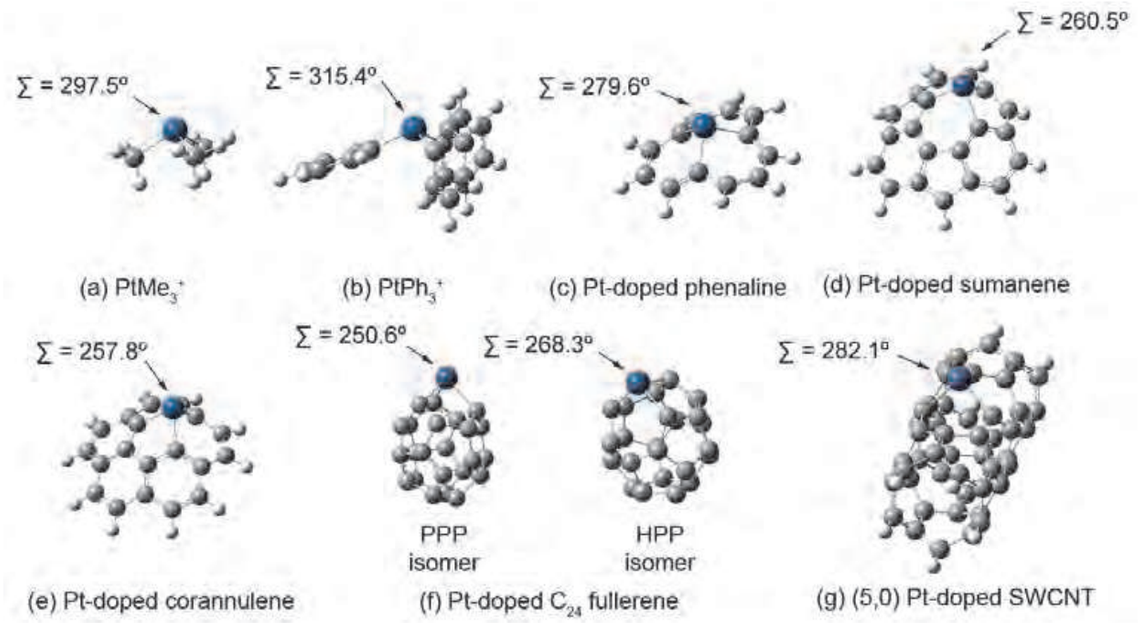

Fig. 4.9. Optimized geometries of model alkyl- and arylplatinum complexes (Yeung et al. 2011).

By means of C≡O vibrational frequency analysis (Table 4-3), we found that Pt-doped (5,5) SWCNTs demonstrated net backdonation to CO (Yeung et al. 2010), while the corresponding (5,0) SWCNT system underwent adsorption with net donation of electron density from the adsorbate (Yeung et al. 2011). In contrast, all other model complexes evaluated have a tendency to deplete electron density from CO. Based on similar stretching frequencies of CO-adsorbed Pt-doped C_{24} and corannulene, higher levels of π-conjugation appear to have a positive impact on the ability to backbond to incoming ligands, leading to a tighter Pt–CO interaction (~2.00 Å). The most acidic complexes, however, are $PtPh_3^+$ and $PtMe_3^+$, which display weaker Pt–CO interactions (~2.11 Å). Based on this investigation, the predicted trend of Lewis acidity is as follows:

(5,0) Pt-doped SWCNT ~ Pt-doped corannulene < Pt-doped C_{24} PPP isomer < Pt-doped C_{24} HPP isomer < Pt-doped sumanene < Pt-doped phenaline < $PtPh_3^+$ < $PtMe_3^+$.

By means of NMR analysis (Table 4-4), we were surprised to observe decreased chemical shifts of the β-H of coordinated MA in both (5,0) Pt-doped SWCNT and Pt-doped corannulene, implying that the charge-separated resonance structure is less important than in uncoordinated MA. This effect can be attributed to larger steric hindrance toward the productive coordination of the C=O group of MA and the Pt atom. All other complexes are in fact strong Lewis acids ($\Delta\delta$ ~ 0.5 ppm). Lewis acid/Lewis base pair formation decreases the C1−C2 bond length and increases C1=O and C2=C3 bond lengths and suggests that reactivity at C2 and C3 towards electrophiles and nucleophiles, respectively, should be enhanced. Complexation of the model organoplatinum complexes resulted in larger geometric deviations than from the simpler $PtMe_3^+$ and $PtPh_3^+$ systems and suggests that higher levels of π-curvature and increased ability to favor delocalization of the electron density may facilitate this productive interaction. The trend of Lewis acidity suggested by

chemical shift analysis is nonetheless identical to the conclusion derived from the above C≡O vibrational frequency analysis.

Pt complex	**Σ**[a]	***q*(Pt)**[b]	**E_{elec}**[c]	**ΔG**[d]	***d*(Pt−C)**[e]	***d*(C≡O)**[e]	**$\nu_{C\equiv O}$**[f]	***q*(Pt/CO)**[g]	***q*(CO)**[h]
$PtMe_3^+$	297.5°	0.77	−24.0	−8.25	2.116	1.156	2089.3	0.54	0.25
$PtPh_3^+$	315.4°	0.77	−16.8	−0.46	2.113	1.160	2055.1	0.54	0.22
Pt-doped phenaline	279.6°	0.74	−28.6	−13.07	2.057	1.161	2050.3	0.40	0.23
Pt-doped sumanene	260.5°	0.77	−35.2	−19.67	2.025	1.163	2043.4	0.39	0.21
Pt-doped corannulene	257.8°	0.59	−34.3	−18.22	1.983	1.179	1949.4	0.26	0.08
Pt-doped C_{24} PPP	250.6°	0.69	−31.6	−16.74	2.027	1.167	2017.3	0.32	0.17
Pt-doped C_{24} HPP	268.3°	0.66	−32.7	−17.59	1.995	1.166	2026.4	0.30	0.22
(5,0) Pt-doped SWCNT	292.2°	0.53	−36.0	−20.31	1.971	1.179	1949.8	0.12	0.12

[a]Sum of angles around Pt center (without adsorbate).
[b]Partial charge on Pt atom (without adsorbate).
[c]Electronic energy of stabilization (in kcal/mol) upon CO adsorption.
[d]Free energy of stabilization (in kcal/mol) upon CO adsorption at 298 K.
[e]Bond length (in Å).
[f]Vibration frequency (in cm^{-1}) of bound C≡O molecule (*cf*. 2028.8 cm^{-1} for unbound free CO).
[g]Partial charge of Pt atom in CO-adsorbed Pt complex.
[h]Partial charge on bound CO molecule.

Table 4.3. Electronic structural data for alkyl- and arylplatinum complexes and their CO-adsorbates (Yeung et al. 2011).

LA/MA complex	***d*(C1=O)**[a]	***d*(C1−C2)**[a]	***d*(C2=C3)**[a]	***q*(O)**[b]	***q*(C3)**[c]	**δ(H)**[d]	**Δδ(H)**[e]
Uncoordinated MA	1.223	1.499	1.351	−0.496	−0.250	6.25	0.00
$PtMe_3^+$/MA	1.248	1.488	1.354	−0.583	−0.215	7.02	0.77
$PtPh_3^+$/MA	1.243	1.488	1.354	−0.557	−0.221	6.94	0.69
Pt-doped phenaline/MA	1.249	1.486	1.356	−0.584	−0.229	6.80	0.55
Pt-doped sumanene/MA	1.249	1.484	1.356	−0.577	−0.221	6.71	0.46
Pt-doped corannulene/MA	1.278	1.440	1.384	−0.643	−0.311	5.53	−0.72
Pt-doped C_{24} PPP/MA	1.254	1.472	1.363	−0.595	−0.266	6.30	0.05
Pt-doped C_{24} HPP/MA	1.245	1.479	1.359	−0.552	−0.250	6.39	0.14
(5,0) Pt-doped SWCNT/MA	1.276	1.441	1.385	−0.636	−0.317	5.62	−0.63

[a]Bond length (in Å).
[b]Partial charge on O atom.
[c]Partial charge on C3 atom.
[d]Chemical shift (in ppm) on H atom (referenced to tetramethylsilane).
[e]Difference in chemical shift (in ppm) on H atom relative to uncoordinated maleic anhydride (referenced to tetramethylsilane).

Table 4.4. Electronic structural data for Lewis acid/maleic anhydride complexes (Yeung et al. 2011)

By means of enhancing the reactivity of chemical reactions such as the Diels-Alder cycloaddition, we observed a surprising *decrease* in reaction efficiency (Table 4-5) when employing the (5,0) Pt-doped SWCNT as a catalyst (Figure 4-10). While our vibrational frequency and NMR analyses both suggested rate enhancements, this was not the case for our nanotube-based catalyst. This suggests that although the LUMO energy of the dienophile (MA) was decreased by binding, the steric demand for the productive [4+2] cycloaddition made catalysis less likely. In agreement with the literature (Hsieh et al. 2007), we determined that $PtMe_3^+$ is a viable catalyst for the Diels-Alder reaction in addition to the other model Pt complexes. The Lewis acid catalyzed cycloaddition of MA and CPD varied inversely in efficiency with catalyst bulk. Of note, while Pt-doped fullerene gave an approximate threefold increase in rate, other systems yielded greater enhancements of up to 10^7-fold! Pyramidalization of the carbon framework has relatively little impact on the effectiveness of the proposed catalysis.

The cyclohexene product formed in the Diels-Alder cycloaddition can exist as one of two diastereomeric compounds (Rulisek et al. 2005; Dewar & Pierini 1984). The so-called *endo* product is *kinetically* favored and involves *secondary orbital interactions* between the two unreactive C atoms on the diene (CPD) and the π-orbitals of the neighboring C=O groups on the alkene (MA). The *exo* product is accessible through thermodynamic control. In our studies, if we assume kinetic control of the Diels-Alder reaction, Pt complexes with higher levels of delocalization of electron density in the catalyst tend to give a lower preference for the *endo* product. To our delight, while Pt-doped SWCNTs were not excellent catalysts for this transformation, the *exo* product became favored over the *endo* product (Yeung et al. 2011). This result suggests that nanocatalysts have the potential to effect *complementary* selectivities to other traditional catalysts. By controlling externally applied voltages, the Lewis acidity of transition metal dopants can be manipulated, hence providing an opportunity for tuning the efficiency and selectivity of nanocatalyzed reactions. The advantage of using nanomaterials in catalysis is that they sit uniquely at the boundary between homogeneous and heterogeneous catalysis. This provides organic chemists an opportunity to establish the connection between reaction mechanisms of these two catalytic systems. In addition, substitutional doping of CNTs with Pt atoms may be a useful and effective strategy for developing heterogeneous-like Lewis acid catalysts. Immobilization of reactive Lewis acids is expected to ease catalyst recovery and reuse of precious metals, as well as afford an enhanced stability of these reactive species. Moreover, we can possess greater controllability of the reaction process, e.g., to pause the reaction by simply separating the catalyst from the solution. Other transformations may be catalyzed by our HSWCNTs, such as Mukaiyama aldol reactions, and should be explored both theoretically and experimentally.

More complex, novel nanosystems may even become possible. Because nanotubes are channels, we may one day be able to achieve nanoscale microfluidics. We can imagine a transition metal-doped SWCNT embedded within a much larger SWCNT. If this is possible, the nanochannels sitting between the two carbon backbones may provide enhanced chemical reactivity due to higher local concentrations of the reactive partners. In the ideal world, it may be possible that reactants be introduced at one end of a nanochannel and products come out of the other end. Cooperative catalysis between different transition metals may allow for unique types of catalysis that are not possible in bulk solutions, on flat surfaces, or at pointy small clusters. Needless to say, nanocatalysis remains an emerging field that will continue to develop in the years to come.

Catalyst	$\Delta G_{exo}^{\ddagger a}$	$\Delta G_{exo}{}^{b}$	$\Delta G_{endo}^{\ddagger c}$	$\Delta G_{endo}{}^{d}$	$\Delta\Delta G^{\ddagger e}$	$k_{endo}/k_{exo}{}^{f}$	$k_{cat}/k_{uncat}{}^{g}$
none	27.3	−3.8	26.7	−3.0	0.6	2.78	1.00
$PtMe_3^+$	15.9	−8.1	14.4	−9.5	1.4	11.43	1.27×10^3
$PtPh_3^+$	17.4	−8.2	16.8	−8.5	0.6	2.79	1.58×10^3
Pt-doped phenaline	17.7	−8.2	16.7	−7.7	1.0	5.60	1.47×10^3
Pt-doped sumanene	16.8	−8.6	16.2	−8.4	0.6	2.63	3.01×10^3
Pt-doped corannulene	16.0	−13.3	15.3	−13.3	0.7	3.43	8.22×10^6
Pt-doped C_{24} PPP	23.5	−4.0	22.6	−3.5	0.9	4.26	1.42
Pt-doped C_{24} HPP	23.5	−4.5	22.5	−4.2	1.0	5.44	2.99
(5,0) Pt-doped SWCNT	31.0	6.4	31.9	6.5	–0.9	0.21	1.6×10^{-3}

[a]Free energy required to reach transition state leading to *exo* product at 298 K.
[b]Free energy change to *exo* product at 298 K.
[c]Free energy required to reach transition state leading to *endo* product at 298 K.
[d]Free energy change to *endo* product at 298 K.
[e]Difference in free energy changes required to reach transition states leading to *endo* and *exo* products at 298 K.
[f]Relative rate leading to *endo* product versus *exo* product.
[g]Relative rate of catalyzed Diels-Alder reaction versus uncatalyzed Diels-Alder reaction.

Table 4.5. Free energies (in kcal/mol) and rates of the Diels-Alder reaction of maleic anhydride and cyclopentadiene as catalyzed by alkyl- and arylplatinum complexes (Yeung et al. 2011)

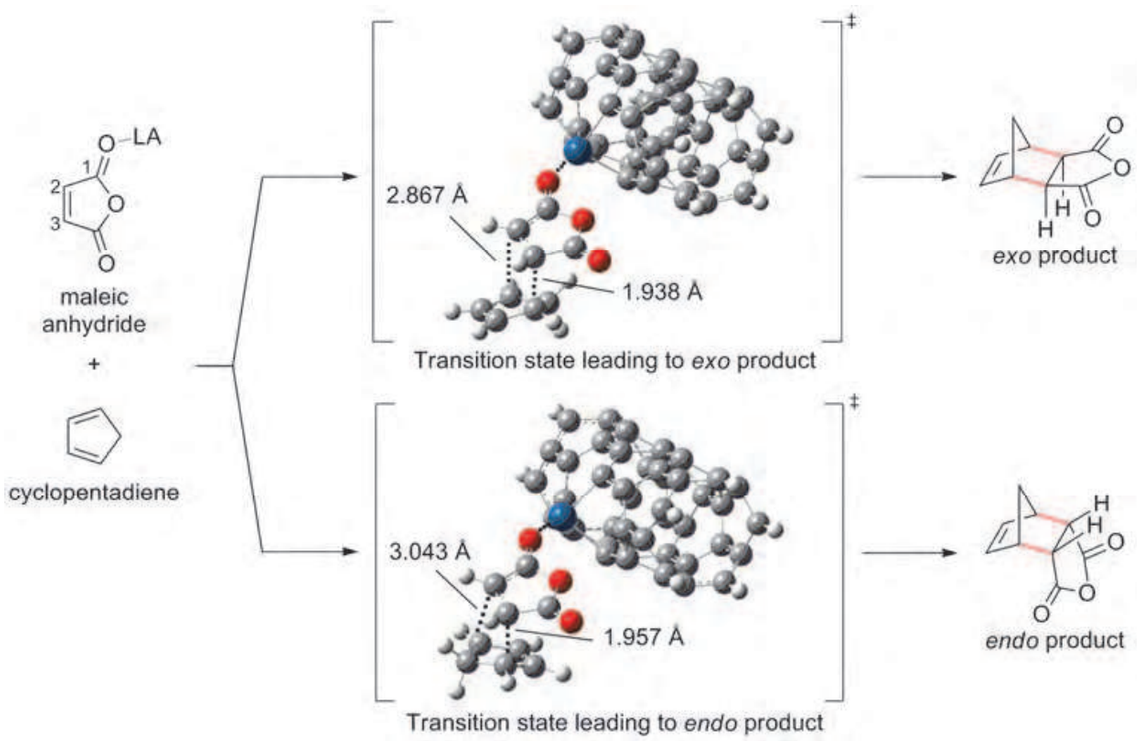

Fig. 4.10. Transition states of the Diels-Alder reaction of maleic anhydride and cyclopentadiene (Yeung et al. 2011). Legend: dark grey = C, light grey = H, red = O, blue = Pt.

5. Concluding remarks

Within DFT, the rich chemistry of substitutionally doped SWCNTs has been investigated. We summarize our findings below:

1. A mono vacancy formed by removing a single C atom from the sidewall of a SWCNT rearranges to form a five-membered carbocycle and a single C atom with a dangling bond (i.e., the 5-1DB defect). 5-1DB defects are reactive with NO, liberating NO_2 and N-doped SWCNTs, and with O_3, generating O_2 and O-doped SWCNTs.
2. Substitutional doping of SWCNTs with transition metals results in buckling of the nanotube sidewall with the larger atom protruding to the exterior.
3. Adsorption of gases onto Pt-doped SWCNTs is analogous to the coordination chemistry of monomeric Pt complexes. Because the nanotube sidewall provides much larger steric bulk, multiple adsorption is thermodynamically unfavorable. The ability for Pt atoms to perform physisorption and chemisorption depends strongly on the doping location. Adsorption results in a change in the electronic structure of Pt-doped SWCNTs.
4. Pt-doped SWCNTs exhibit Lewis acidity similar to that of simple alkyl- and arylplatinum complexes. Evaluation of Lewis acid strength can be done by measuring the stretching frequency of a bound molecule of CO or by ^{1}H NMR studies of the β-H of Lewis acid/Lewis base complexes formed with a,β-unsaturated carbonyl compounds. However, because the nanotube provides larger steric bulk than simple alkyl- and arylplatinum complexes, the ability to activate a substrate for conventional catalysis may be impeded, but alternative catalytic activities might be released instead.

Transition metal-doped SWCNTs have yet to be prepared experimentally. In this Chapter, we have provided a comprehensive overview of the potential of these nanomaterials and their applications in nanosensing, nanoelectronics, and nanocatalysis. Our initial investigations here should provide inspiration and guidance to experimentalists in their own endeavors.

6. Acknowledgements

We thank the Natural Sciences and Engineering Research Council (NSERC) of Canada for financial support. WestGrid and C-HORSE have provided the necessary computational resources. C.S.Y. gratefully acknowledges NSERC for an Undergraduate Student Research Award.

7. References

Ajayan, P. M., Ravikumar, V. & Charlier, J.-C. (1998) Surface reconstructions and dimensional changes in single-walled carbon nanotubes. *Phys. Rev. Lett.*, *81*, 1437-1440.

Ajayan, P. M. (1999) Nanotubes from carbon. *Chem. Rev.*, *99*, 1787-1800.

Avouris, P., Freitag, M. & Perebeinos, V. (2008) Carbon-nanotube photonics and optoelectronics. *Nature Photonics*, *2*, 341-350.

Backus, E. H. G., Eichler, A., Grecea, M. L., Kleyn, A. W. & Bonn, M. (2004) Adsorption and dissociation of NO on stepped Pt (533). *J. Chem. Phys.*, *121*, 7946-7954.

Becke, A. D. (1988) Density-functional exchange-energy approximation with correct asymptotic-behavior. *Phys. Rev. A*, *38*, 3098-3100.

Berber, S. & Oshiyama, A. (2006) Reconstruction of mono-vacancies in carbon nanotubes: atomic relaxation vs. spin polarization. *Physica B*, *376-377*, 272-275.

Bethune, D. S., Kiang, C. H., de Vries, M. S., Gorman, G., Savoy, R., Vazquez, J. & Beyers, R. (1993) Cobalt-catalyzed growth of carbon nanotubes with single-atomic-layer walls. *Nature*, *363*, 605-607.

Boulikas, T. & Vougiouka, M. (2003) Cisplatin and platinum drugs at the molecular level. *Oncol. Rep.*, *10*, 1663-1682.

Branz, W., Billas, I. M. L., Malinowski, N., Tast, F., Heinebrodt, M. & Martin, T. P. (1998) Cage substitution in metal-fullerene clusters. *J. Chem. Phys.*, *109*, 3425-3430.

Bryning, M. B., Islam, M. F., Kikkawa, J. M. & Yodh, A. G. (2005) Very low conductivity threshold in bulk isotropic single-walled carbon nanotube-epoxy composites. *Adv. Mater.*, *17*, 1186-1191.

Buzea, C., Blandino, I. I. P. & Robbie, K. (2007) Nanomaterials and nanoparticles: sources and toxicity. *Biointerphases*, *2*, MR17-MR172.

Caruso, E. B., Petralia, S., Conoci, S., Giuffrida, S. & Sortino, S. (2007) Photodelivery of nitric oxide from water-soluble platinum nanoparticles. *J. Am. Chem. Soc.*, *129*, 480-481.

Changgeng, D., Jinlong, Y., Rongsheng, H. & Kelin, W. (2001) Formation mechanism and structural and electronic properties of metal-substituted fullerenes $C_{69}M$ (M = Co, Rh, and Ir). *Phys. Rev. A.*, *64*, 043201.

Chen, Y. K., Liu, L. V. & Wang, Y. A. (2010) Density functional study of interaction of atomic Pt with pristine and Stone-Wales-defective single-walled boron nitride nanotubes. *J. Phys. Chem. C*, *114*, 12382-12388.

Chen, Y. K.; Liu, L. V., Tian, W. Q. & Wang, Y. A. (2011) Theoretical studies of transition-metal-doped single-walled carbon nanotubes. *J. Phys. Chem. C*, *115*, 9306-9311.

Chiaretti, M., Mazzanti, G., Bosco, S., Bellucci, S., Cucina, A., le Foche, F., Carru, G. A., Mastrangelo, S., di Sotto, A., Masciangelo, R., Chiaretti, A. M., Balasubramanian, C., de Bellis, G., Micciulla, F., Porta, N., Deriu, G. & Tiberia, A. (2008) Carbon nanotubes toxicology and effects on metabolism and immunological modification in vitro and in vivo. *J. Phys.*: *Condens. Matter*, *20*, 474203.

Chico, L., Santos, H., Ayuela, A., Jaskolski, W., Pelc, M. & Brey, L. (2010) Unzipped and defective nanotubes: rolling up graphene and unrolling tubes. *Acta Phys. Polonica A*, *118*, 433-441.

Childs, R. F., Mulholland, D. L. & Nixon, A. (1982) The Lewis acid complexes of α,β-unsaturated carbonyl and nitrile compounds. A nuclear magnetic resonance study. *Can. J. Chem.*, *60*, 801-808.

Chopra, S., Pham, A., Gaillard, J., Parker, A. & Rao, A. M. (2002) Carbon-nanotube-based resonant-circuit sensor for ammonia. *Appl. Phys. Lett.*, *80*, 4632-4634.

Collins, P. G., Bradley, K., Ishigami, M. & Zetti, A. (2000) Extreme oxygen sensitivity of electronic properties of carbon nanotubes. *Science*, 287, 1801-1804.

Collins, P. G. (2010) Defects and disorder in carbon nanotubes, *in* The Oxford Handbook of Nanoscience and Nanotechnology, Oxford University Press: New York, NY, Volume 2, Chapter 2, pp. 31-93.

Culotta, E. & Koshland Jr., D. E. (1992) NO news is good news. *Science*, *258*, 1862-1865.

Dapprich, S., Komaromi, I., Byun, K. S., Morokuma, K. & Frisch, M. J. (1999) A new ONIOM implementation in Gaussian 98. 1. The calculation of energies, gradients and vibrational frequencies and electric field derivatives. *J. Mol. Struc. (Theochem)*, *462*, 1-21.

Dewar, M. J. S. & Pierini, A. B. (1984) Mechanism of the Diels-Alder reaction. Studies of the addition of maleic anhydride to furan and methylfurans. *J. Am. Chem. Soc.*, *106*, 203-208.

Dewar, M. J. S., Zoebisch, E. G. & Healy, E. F. (1985) AM1: A new general purpose quantum mechanical molecular model. *J. Am. Chem. Soc.*, *107*, 3902-3909.

Ditchfield, R., Hehre, W. J. & Pople, J. A. (1971) Self-consistent molecular orbital methods. 9. Extended Gaussian-type basis for molecular-orbital studies of organic molecules. *J. Chem. Phys.*, *54*, 724.

Dunning Jr., T. H. & Hay, P. J. (1976) Gaussian basis sets for molecular calculations, *in* Modern Theoretical Chemistry, Plenum: New York, NY, Volume 3, pp. 1-28.

Ewels, C., Glerup, M. & Krstic, V. (2010) Nitrogen and boron doping in carbon nanotubes, *in* Doped Nanomaterials and Nanodevices, American Scientific Publishers: Valencia, CA, Volume 3.

Frisch, M. J., Trucks, G. W., Schlegel, H. B., Scuseria, G. E., Robb, M. A., Cheeseman, J. R., Montgomery, J. A., Vreven, T., Kudin, K. N., Burant, J. C., Milliam, J. M. Iyengar, S. S., Tomasi, J., Barone, V., Mennucci, B., Cossi, M. , Scalmani, G., Rega, N., Petersson, G. A., Nakatsuji, H., Hada, M. Ehara, M., Toyota, K., Fukuda, R., Hasegawa, J., Ishida, M., Nakajima, T., Honda, Y., Kitao, O., Nakai, H., Li, X., Knox, J. E., Hratchian, H. P., Cross, J. B., Bakken, V., Adamo, C., Jaramillo, J., Gomperts, R., Stratmann, R. E., Yazyev, O., Austin, A. J., Cammi, R., Pomelli, C., Ochterski, J. W., Ayala, P. Y., Morokuma, K., Voth, G. A., Salvador, P., Dannenberg, J. J. Zakrzewski, V. G., Dapprich, S., Daniels, A. D., Farkas, O., Malick, D. K., Rabuck, A. D., Raghavachari, K., Foresman, J. B., Ortiz, J. V., Cui, Q., Baboul, A. G., Clifford, S., Coislowski, J., Stefanov, B. B., Liu, G., Liashenko, A., Piskorz, P., Komaromi, I., Martin, R. L., Fox, D. J., Keith, T., Al-Laham, M. A., Peng, C. Y., Nanayakkara, A., Challacombe, M., Gill, P. M. W., Johnson, B., Chen, W., Wong, M. W., Gonzalez, C. & Pople, J. A. (2003) Gaussian 03, Revision B.05, Gaussian, Inc.: Wallingford CT.

Fuhrer, M. S. (2003) Single-walled carbon nanotubes for nanoelectronics, *in* Advanced Semiconductor and Organic Nano-Techniques (Part II), Academic Press: London, Chapter 6, pp. 293-343.

Fukui, K. (1982) Role of frontier orbitals in chemical reactions. *Science*, *218*, 747-754.

Gayathri, V. & Geetha, R. (2007) Hydrogen adsorption in defected carbon nanotubes. *Adsorption*, *13*, 53-59.

Golberg, D., Bando, Y., Huang, Y., Terao, T., Mitome, M., Tang, C. & Zhi, C. (2010) Boron nitride nanotubes and nanosheets. *ACS Nano*, *4*, 2979-2993.

Glerup, M., Krstic, V., Ewels, C., Holzinger, M. & Lier, G. V. (2010) Doping of carbon nanotubes, *in* Doped Nanoamterials and Nanodevices, American Scientific Publishers: Valencia, Volume 3.

Griffith, O. W. & Stuehr, D. J. (1995) Nitric oxide synthases: properties and catalytic mechanism. *Ann. Rev. Physiol.*, *57*, 707-736.

Grinvald, A. & Hildesheim, R. (2004) VSDI: a new era in functional imaging of cortical dynamics. *Nature Rev. Neurosci.*, *5*, 874-885.

Haddon, R. C. & Scott, L. T. (1986) π-Orbital conjugation and rehybridization in bridged annulenes and deformed molecules in general: π-orbital axis vector analysis. *Pure Appl. Chem.*, *58*, 137-142.

Hay, P. J. & Wadt, W. R. (1985) Ab initio effective core potentials for molecular calculations – potentials for K to Au including the outermost core orbitals. *J. Chem. Phys.*, *82*, 299-310.

Hsieh, V., de Crisci, A. G., Lough, A. J. & Fekl, U. (2007) Lewis-acidity of trimethylplatinum(IV) with labile oxygen-donor ligands. *Organometallics*, *26*, 938-944.

Hu, C. & Hu, S. (2009) Carbon nanotube-based electrochemical sensors: principles and applications in biomedical systems. *J. Sensors*, *2009*, 187615.

Iijima, S. (1991) Helical microtubules of graphitic carbon. *Nature*, *354*, 56-58.
Iijima, S. & Ichihashi, T. (1993) Single-shell carbon nanotubes of 1-nm diameter. *Nature*, *363*, 603-605.
Javey, A., Guo, J., Wang, Q., Lundstrom, M. & Dai, H. (2003) Ballistic carbon nanotube field-effect transistors. *Nature*, *424*, 654-657.
Karakoti, A. S., Hench, L. L. & Seal, S. (2006) The potential toxicity of nanomaterials – the role of surfaces. *JOM*, *58*, 77-82.
Karousis, N., Tagmatarchis, N. & Tasis, D. (2010) Current progress on the chemical modification of carobn nanotubes. *Chem. Rev.*, *110*, 5366-5397.
Kong, J., Franklin, N. R., Zhou, C., Chapline, M. G., Peng, S., Cho, K. & Dai, H. (2000) Nanotube molecular wires as chemical sensors. *Science*, *287*, 622-625.
Kong, J., Chapline, M. G. & Dai, H. (2001) Functionalized carbon nanotubes for molecular hydrogen sensors. *Adv. Mater.*, *13*, 1384-1386.
Kong, Q., Zhuang, J., Xu, J., Shen, Y., Li, Y., Zhao, L. & Cai, R. (2003) Contrasting behaviors of metal fullerides $C_{60}Rh_x$ and $C_{60}M_x$ (M = La, Y) in the metallofullerrene formation by laser ablation. *J. Phys. Chem. A*, *107*, 3670-3677.
Kuczkowski, R. L. (1992) The structure and mechanism of formation of ozonides. *Chem. Soc. Rev.*, *21*, 79-83.
Lam, C.-W., James, J. T., McCluskey, R., Arepalli, S. & Hunter, R. L. (2006) A review of carbon nanotube toxicity and assessment of potential occupational and environmental health risks. *Crit. Rev. Toxicol.*, *36*, 189-217.
Laszlo, P. & Teston, M. (1990) Determination of the acidity of Lewis acids. *J. Am. Chem. Soc.*, *112*, 8750-8754.
Lee, C., Yang, W. & Parr, R. G. (1988) Development of the Colle-Salvetti correlation-energy formula into a functional of the electron density. *Phys. Rev. B*, *37*, 785-789.
Li, C., Thostenson, E. T. & Chou, T.-W. (2008) Sensors and actuators based on carbon nanotubes and their composites: a review. *Compos. Sci. Technol.*, *68*, 1227-1249.
Li, J., Lu, Y., Ye, Q., Cinke, M., Han, J. & Meyyappan, M. (2003) Carbon nanotube sensors for gas and organic vapor detection. *Nano Lett.*, *3*, 929-933.
Li, J., Jia, G. & Zhang, Y. (2007) Chemical anisotropies of carbon nanotubes and fullerenes caused by the curvature directivity. *Chem. Eur. J.*, *132*, 6430-6436.
Li, X. M., Tian, W. Q., Huang, X.-R., Sun, C.-S. & Jiang, L. (2009) Adsorption of hydrogen on novel Pt-doped BN nanotubes. *J. Molec. Struc.: THEOCHEM*, *901*, 103-109.
Liu, L. V., Tian, W. Q. & Wang, Y. A. (2006) Chemical reaction of nitric oxides with the 5-1DB defect of the single-walled carbon nanotube. *J. Phys. Chem. B*, *110*, 1999-2005.
Liu, L. V., Tian, W. Q. & Wang, Y. A. (2006a) Ozonization at the vacancy defect site of the single-walled carbon nanotube. *J. Phys. Chem. B*, *110*, 13037-13044.
Liu, L. V., Tian, W. Q. & Wang, Y. A. (2009) Ab initio studies of vacancy-defected fullerenes and single-walled carbon nanotubes. *Int. J. Quantum Chem.*, *109*, 3441-3456.
Lu, X. & Chen, Z. (2005) Curved pi-conjugation, aromaticity, and the related chemistry of small fullerenes ($<C_{60}$) and single-walled carbon nanotubes. *Chem. Rev.*, *105*, 3643-3696.
Menzel, L., Kosterev, A. A., Curl, R. F., Tittel, F. K., Gmachi, C., Capasso, F., Sivco, D. L., Baillargeon, J. N., Hutchinson, A. L, Cho, A. Y. & Urban, W. (2001) Spectroscopic determination of biological NO with a quantum cascade laser. *Appl. Phys. B*, *72*, 859-863.
Miller, M. R. & Megson, I. L. (2007) Recent developments in nitric oxide donor drugs. *Br. J. Pharmacol.*, *151*, 305-321.

Moniruzzaman, M. & Winey, K. I. (2006) Polymer nanocomposites containing carbon nanotubes. *Macromolecules*, *39*, 5194-5205.

Nel, A., Xia, T., Maedler, L. & Li, N. (2006) Toxic potential of materials at the nanolevel. *Science*, *311*, 622-627.

Nevidomskyy, A. H., Csanyi, G. & Payne, M. C. (2003) Chemically active substitutional nitrogen impurity in carbon nanotubes. *Phys. Rev. Lett.*, *91*, 105502.

Oberdorster, G., Stone, V. & Donaldson, K. (2007) Toxicology of nanoparticles: a historical perspective. *Nanotoxicology*, *1*, 2-25.

Orita, H., Itoh, N. & Inada, Y. (2004) All electron scalar relativistic calculations on adsorption of CO on Pt(111) with full-geometry optimization: a correct estimation for CO site-preference. *Chem. Phys. Lett.*, *384*, 271-276.

Park, J.-Y. (2004) Nanoelectronics/mechanics with carbon nanotubes. http://nanohub.org/resources/157.

Peng, S. & Cho, K. (2003) Ab initio study of doped carbon nanotube sensors. *Nano Lett.*, *3*, 513-517.

Perdew, J. P., Burke, K. & Ernzerhof, M. (1996) Generalized gradient approximation made simple. *Phys. Rev. Lett.*, *77*, 3865-3868.

Perdew, J. P., Burke, K. & Wang, Y. (1996a) Generalized gradient approximation for the exchange-correlation hole of a many-electron system. *Phys. Rev. B*, *54*, 16533-16539.

Poblet, J. M., Munoz, J., Winkler, K., Cancilla, M., Hayashi, A., Lebrilla, C. B., Balch, A. L. & Winkler, K. (1999) Geometric and electronic structure of metal-caged fullerenes, $C_{59}M$ (M = Pt, Ir) obtained by laser ablation of electrochemically deposited films. *Chem. Commun.*, 493-494.

Procelewska, J., Zahl, A., Liehr, G., van Eldik, R., Smythe, N. A., Williams, B. S. & Goldberg, K. I. (2005) Mechanistic information on the reductive elimination from cationic trimethylplatinum(IV) complexes to form carbon-carbon bonds. *Inorg. Chem.*, *44*, 7732-7742.

Rappe, A. K., Casewit, C. J., Colwell, K. S., Goddard III, W. A. & Skiff, W. M. (1992) UFF, a full periodic-table force-field for molecular mechanics and molecular-dynamics simulations. *J. Am. Chem. Soc.*, *114*, 10024-10035.

Reed, A. E., Curtiss, L. A. & Weinhold, F. (1988) Intermolecular interactions from a natural bond orbital, donor-acceptor viewpoint. *Chem. Rev.*, *88*, 899-926.

Rouxinol, F. P., Gelamo, R. V. & Moshkalev, S. A. (2010) Gas sensors based on decorated carbon nanotubes, *in* Carbon Nanotubes. InTech, Chapter 19, pp. 357-374.

Rulisek, L., Sebek, P., Havlas, Z., Hrabal, R., Capek, P. & Svatos, A. (2005) An experimental and theoretical study of stereoselectivity of furan-maleic anhydride and furan-maleimide Diels-Alder reactions. *J. Org. Chem.*, *70*, 6295-6302.

Schipper, M. L., Nakayama-Ratchford, N., Davis, C. R., Kam, N. W. S., Chu, P., Liu, Z., Sun, X., Dai, H. & Gambhir, S. S. (2008) A pilot toxicology study of single-walled carbon nanotubes in a small sample of mice. *Nature Nanotech.*, *3*, 216-221.

Schlegel, H. B., Millam, J. M., Iyengar, S. S., Voth, G. A., Scuseria, G. E., Daniels, A. D. & Frisch, M. J. (2001) Ab initio molecular dynamics: propagating the density matrix with Gaussian orbitals. *J. Chem. Phys.*, *114*, 9758-9763.

Serp, P., Corrias, M., & Kalck, P. (2003) Carbon nanotubes and nanofibers in catalysis. *Appl. Catal. A*, *253*, 337-358.

Singh, R., Pantarotto, D., Lacerda, L., Pastorin, G., Klumpp, C., Prato, M., Bianco, A. & Kostarelos, K. (2006) Tissue biodistribution and blood clearance rates of intravenously administered carbon nanotube radiotracers. *Proc. Natl. Acad. Sci. U.S.A.*, *103*, 3357-3362.

Sinha, N., Ma, J. & Yeow, J. T. W. (2006) Carbon nanotube-based sensors. *J. Nanosci. Nanotech.*, *6*, 573-590.

Sonia, K. & Niranjan, M. (2010) Quantum conductance of defected carbon nanotubes. *AIP Conf. Proc.*, *1324*, 415-418.

Sparta, M., Borve, K. J. & Jensen, V. R. (2006) Structure and stability of networked metallofullerenes of the transition metals. *J. Phys. Chem. A*, *110*, 11711-11716.

Srivastava, D., Chenyu, W. & Cho, K. (2003) Nanomechanics of carbon nanotubes and composites. *Appl. Mech. Rev.*, *56*, 215-230.

Srivastava, D., Menon, M., Daraio, C., Jin, S., Sadanadan, B. & Rao, A. M. (2004) Vacancy-mediated mechanism of nitrogen substitution in carbon nanotubes. *Phys. Rev. B*, *69*, 153414.

Stewart, J. J. P. (1989) Optimization of parameters for semiempirical methods. I. Method. *J. Comput. Chem.*, *10*, 209-220.

Stone, A. J. & Wales, D. J. (1986) Theoretical studies of icosahedral footballene sixty-carbon-atom molecules and some related species. *Chem. Phys. Lett.*, *128*, 501-503.

Tasis, D., Tagmatarchis, N., Bianco, A. & Prato, M. (2006) Chemistry of carbon nanotubes. *Chem. Rev.*, *106*, 1105-1136.

Tenderholt, A. (2005) *PyMOlyze*, Version 1.1.

Tian, W. Q., Liu, L. V. & Wang, Y. A. (2006) Electronic properties and reactivity of Pt-doped carbon nanotubes. *Phys. Chem. Chem. Phys.*, *8*, 3528-3539.

Tsukagoshi, K., Yoneya, N., Uryu, S., Aoyagi, Y., Kanda, A., Ootuka, Y. & Alphenaar, B. W. (2002) Carbon nanotube devices for nanoelectronics. *Physica B*, *323*, 107-114.

Wang, J., Lee, C. H. & Yap, Y. K. (2010) Recent advances in boron nitride nanotubes. *Nanoscale*, *2*, 2028-2034.

Wang, Y. & Yeow, J. T. W. (2009) A review of carbon nanotubes-based gas sensors. *J. Sensors*, 493904.

Wheatley, P. S., Butler, A. R., Crane, M. S., Fox, S., Xiao, B., Rossi, A. G., Megson, I. L. & Morris, R. E. (2006) NO-releasing zeolites and their antithrombotic properties. *J. Am. Chem. Soc.*, *128*, 502-509.

White, C. T. & Todorov, T. N. (1998) Carbon nanotubes as long ballistic conductors. *Nature*, *393*, 240-242.

Wolinski, K., Hilton, J. F. & Pulay, P. (1990) Efficient implementation of the gauge-independent atomic orbital method for NMR chemical shift calculations. *J. Am. Chem. Soc.*, *112*, 8251-8260.

Yang, S. H., Shin, W. H., Lee, J. W., Kim, S. Y., Woo, S. I. & Kang, J. K. (2006) Interaction of a transition metal atom with intrinsic defects in single-walled carbon nanotubes. *J. Phys. Chem. B*, *110*, 13941-13946.

Yao, Y. (2010) Hydrogen storage using carbon nanotubes *in* Carbon Nanotubes, InTech, Chapter 28, pp. 543-562.

Yeung, C. S., Liu, L. V. & Wang, Y. A. (2007) Novel nanotube-coordinated platinum complexes. *J. Comput. Theor. Nanosci.*, *4*, 1108-1119.

Yeung, C. S., Liu, L. V. & Wang, Y. A. (2008) Adsorption of small gas molecules onto Pt-doped single-walled carbon nanotubes. *J. Phys. Chem. C*, *112*, 7401-7411.

Yeung, C. S. & Wang, Y. A. (2011) Lewis acidity of Pt-doped buckybowls, fullerenes, and single-walled nanotubes. *J. Phys. Chem. C*, *115*, 7153-7163.

Zhuang, H. L., Zheng, G. P. & Soh, A. K. (2008) Interactions between transition metals and defective carbon nanotubes. *Comput. Mater. Sci.*, *43*, 823-828.

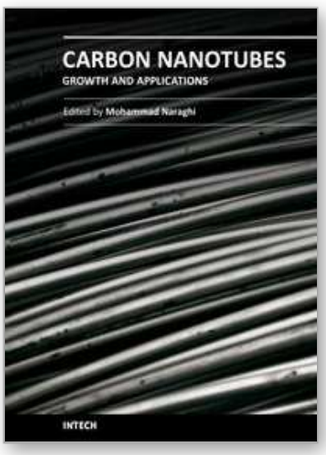

Carbon Nanotubes - Growth and Applications

Edited by Dr. Mohammad Naraghi

ISBN 978-953-307-566-2
Hard cover, 604 pages
Publisher InTech
Published online 09, August, 2011
Published in print edition August, 2011

Carbon Nanotubes are among the strongest, toughest, and most stiff materials found on earth. Moreover, they have remarkable electrical and thermal properties, which make them suitable for many applications including nanocomposites, electronics, and chemical detection devices. This book is the effort of many scientists and researchers all over the world to bring an anthology of recent developments in the field of nanotechnology and more specifically CNTs. In this book you will find:
- Recent developments in the growth of CNTs
- Methods to modify the surfaces of CNTs and decorate their surfaces for specific applications
- Applications of CNTs in biocomposites such as in orthopedic bone cement
- Application of CNTs as chemical sensors
- CNTs for fuelcells
- Health related issues when using CNTs

How to reference

In order to correctly reference this scholarly work, feel free to copy and paste the following:

Charles See Yeung, Ya Kun Chen and Yan Alexander Wang (2011). Defected and Substitutionally Doped Nanotubes: Applications in Biosystems, Sensors, Nanoelectronics, and Catalysis, Carbon Nanotubes - Growth and Applications, Dr. Mohammad Naraghi (Ed.), ISBN: 978-953-307-566-2, InTech, Available from: http://www.intechopen.com/books/carbon-nanotubes-growth-and-applications/defected-and-substitutionally-doped-nanotubes-applications-in-biosystems-sensors-nanoelectronics-and

INTECH
open science | open minds

InTech Europe
University Campus STeP Ri
Slavka Krautzeka 83/A
51000 Rijeka, Croatia
Phone: +385 (51) 770 447
Fax: +385 (51) 686 166
www.intechopen.com

InTech China
Unit 405, Office Block, Hotel Equatorial Shanghai
No.65, Yan An Road (West), Shanghai, 200040, China
中国上海市延安西路65号上海国际贵都大饭店办公楼405单元
Phone: +86-21-62489820
Fax: +86-21-62489821

IntechOpen